의학박사 학위논문

# Comparison of $^{64}$Cu-GUL and $^{64}$Cu-Albumin-GUL by PET Image-based Biodistribution and Absorbed Dose Measurements

# PET 영상 기반 생체 분포 및 흡수 선량 측정을 통한 $^{64}$Cu-GUL 와 $^{64}$Cu-Albumin-GUL 의 비교

2019년 8월

서울대학교 융합과학기술대학원
분자의학 및 바이오제약학과
이은성

의학박사 학위논문

# PET 영상 기반 생체 분포 및 흡수 선량 측정을 통한 **$^{64}$Cu-GUL** 와 **$^{64}$Cu-Albumin-GUL** 의 비교

# Comparison of $^{64}$Cu-GUL and $^{64}$Cu-Albumin-GUL by PET Image-based Biodistribution and Absorbed Dose Measurements

2019년 8월

Eun Seong Lee

*Department of Molecular Medicine and Biopharmaceutical Science*

*The Graduate School of Convergence Science and Technology,*

*Seoul National University*

# Abstract

# Comparison of $^{64}$Cu-GUL and $^{64}$Cu-Albumin-GUL by PET Image-based Biodistribution and Absorbed Dose Measurements

Eun Seong Lee

*Department of Molecular Medicine and Biopharmaceutical Science,*

*The Graduate School of Convergence Science and Technology,*

*Seoul National University*

Targeted radionuclide therapy (TRT) targeting prostate-specific membrane antigen (PMSA) has been introduced in the cutting-edge clinical field of prostate cancer therapy. The effectiveness of TRT depends primarily on the total absorbed dose of the tumor and normal tissues. Therefore, available range of radioactivity dose, above the tumor lethal dose and below the maximum safety dose, must be determined as accurately as possible. Due to the various limitations associated with organ level dosimetry, the voxel-based dosimetry has become essential for the assessment of more accurate absorbed dose during TRT. The main purpose of this study is to compare between radiation exposure of PSMA-targeting peptide and albumin-based nanoparticle to the normal tissue using voxel-based dosimetry method.

In this study, PSMA targeting radiolabeled peptide ($^{64}$Cu-GUL) and albumin-based nanoparticle ($^{64}$Cu-albumin-GUL) were synthesized and voxel-based dosimetry was performed with PET/CT images of normal mice using direct GATE MC simulation.

The absorbed doses are higher in mice treated with $^{64}$Cu-albumin-GUL than in mice treated with $^{64}$Cu-GUL in all of the brain, heart wall, lungs, liver and kidneys. $^{64}$Cu-GUL was mainly accumulated in the kidneys and $^{64}$Cu-albumin-GUL were accumulated in the liver. Residence time of $^{64}$Cu-albumin-GUL in the blood was also higher than that of $^{64}$Cu-GUL.

Single peptide $^{64}$Cu-GUL leads higher radiation exposure to the kidneys and albumin-based nanoparticle $^{64}$Cu-albumin-GUL increases overall radiation exposure to the normal tissue due to its long blood circulation, which should be taken into consideration for optimal TRT.

Keywords: voxel-based dosimetry, GATE, $^{64}$Cu-GUL, $^{64}$Cu-albumin-GUL, PET/CT, PSMA

Student Number: 2010-24240

**Contents**

**Abstract**……………………………………………………….…………………1

**Contents**……………………………………….…………………..……..…3

**List of Tables**...…………………………………………...…………...………6

**List of Figures**……………………………………………...………………7

**List of Abbreviations**…………………………………………………….....9

**Introduction**………………………………………………………………....11

*Single peptide vs. albumin nanoparticle for TRT*……………..…………..11

*Voxel dosimetry with PET/CT for TRT*……………………..…………...13

*PSMA targeting TRT for prostate cancer*…………………….……………14

**Purpose**………………………………………………………………………16

**Materials and Methods**…….……………………………………….…………17

*Preparation of* $^{64}$*Cu-PSMA*……………………….……..………..17

*Conjugation of albumin with ADINO-NHS*……………………………….17

*Preparation of albumin-GUL conjugates*…………………………………18

*Preparation of* $^{64}$*Cu-albumin-GUL*…………………………….……….18

*Serum stability test* ……………………………………………………….21

*In vitro competitive binding assay*…………………………………….….21

*Animal PET/CT imaging*……………………………………………….22

*Urine analysis*……………………………....………….………………24

*Phantom PET/CT imaging*……………………………………………..24

*Image reconstruction* ………………………………….……………24

*Measurement of correction factor* …...…………… ………………… …25

*PET image-based biodistribution* …………………………………..……25

*GATE Monte Carlo simulation* …………………………..…………….26

*Voxel-based absorbed dose calculations using GATE MC* ………………27

**Results** …………………………………………………........... .........29

*Radiolabeling of NOTA-GUL and albumin-GUL using click chemistry*….29

*Determination of the conjugation number*……………………………...31

*Serum stability test*………………………………………………..…..…33

*In vitro affinity test*………….. ………………………………………..…..35

*In vivo animal study* …… ………… …………………………………..…37

*Urine analysis*………………………………………………………......40

*PET-image based biodistribution*………..……………………………..43

*Voxel-based absorbed dose*…………………………………….……....…49

**Discussion**…………………………………………………………………58

**Conclusion**…………………………………………………...…………...63

**References**…………………………………………………………..…………64

국문초록…………………………………………………………………..…………72

**List of tables**

Table 1. Residence time (min) in the major organs……………………………….48

Table 2. Voxel-based absorbed dose (mGy/MBq) in the major organs…. ……….54

## List of figures

Figure 1. Schematics of $^{64}$Cu-albumin-GUL synthesis……………………..……..20

Figure 2. Scheme of animal experiment of PET imaging……………….....…….…23

Figure 3. Schematics of GATE MC simulation for absorbed dose estimation at voxel level…………………………………………………………………….…...28

Figure 4. Radiolabeling efficiencies of $^{64}$Cu-GUL and $^{64}$Cu-albumin-GUL……...30

Figure 5. Determination of the conjugation number of albumin-GUL..........……32

Figure 6. Serum stability test…………………………………………………...34

Figure 7. In vitro affinity test…..…………………………………………..…36

Figure 8. In vivo PET results of $^{64}$Cu-GUL…………………….. ……………….38

Figure 9. In vivo PET results of $^{64}$Cu-albumin-GUL……. ……….…………….. 39

Figure 10. Urine TLC results after 1 hr of $^{64}$Cu-GUL injection……...…………..41

Figure 11. Urine TLC after 1 hr of $^{64}$Cu-albumin-GUL injection.………………...42

Figure 12. Biodistribution per organ (%ID)…….............................................44

Figure 13. Biodistribution (%ID/gm)…...…………………………………..…45

Figure 14. Biodistribution (%ID/gm) in the initial 60 minutes…………………...46

Figure 15. Cumulated activity (MBq.sec) (A) and residence time (min) (B)……..47

Figure 16. Representatives of the dose maps (Gy/voxel) by GATE Monte Carlo Simulation…………………………………………………………………………50

Figure 17. Dose rate per organs (mGy/hr) ……………………………….............51

Figure 18. Normalized dose rates (mGy/MBq.hr), expressed as dose rate per unit radioactivity of the administered radiotracers..………..……...………………….52

Figure 19. Normalized dose rates (mGy/MBq.hr) in the initial 60 minutes………53

Figure 20. Comparison of voxel-based absorbed dose (mGy/MBq) in the major organs between two groups………………………………………………..…...…55

Figure 21. Comparison of voxel-based absorbed dose (mGy/MBq) in the major organs within the group of $^{64}$Cu-GUL injection……………………….……..….56

Figure 22. Comparison of voxel-based absorbed dose (mGy/MBq) in the major organs within the group of $^{64}$Cu-albumin--GUL injection………………………..57

## List of abbreviations

| *Full name* | *Abbreviations* |
|---|---|
| TRT | Targeted radionuclide therapy |
| FcRn | Neonatal Fc receptor |
| MC | Monte Carlo |
| $^{64}Cu$ | Copper-64 |
| PSMA | Prostate-specific membrane antigen |
| GUL | Glutamate-Urea-Lysine |
| ITLC-SG | Instant thin layer chromatography-silica gel |
| $N_3$-NHS | 2,5-dioxopyrrolidin-1-yl 4-azidobutanoate |
| ADIBO-NHS | Azadibenzocyclooctyne-NHS ester |
| $N_3$-NOTA | 2,2',2''-(2-(4-(3-(3-azidopropyl)thioureido)benzyl)-1,4,7-triazonane-1,4,7-triyl)triacetic acid |
| PBS | Phosphate buffered saline |
| MALDI TOF/TOF MS | Matrix-assisted laser desorption ionization time of flight/time of flight mass spectrometry |
| PET | Positron emission tomography |
| CT | Computed tomography |
| OSEM | Ordered-subsets expectation maximum |
| SUV | Standardized uptake value |
| VOI | Volume of interest |
| AUC | Area under curve |

| | |
|---|---|
| dosemaps | Dose distribution map |
| DOF | Degree of functionalization |

# Introduction

### *Single peptide vs. albumin nanoparticle for TRT*

Targeted radionuclide therapy (TRT) has great importance for the treatment of various cancers such as lymphoma, neuroendocrine tumors and recently, prostate cancer (1, 2). It is the basis for successful TRT that radiopharmaceuticals reach the lethal dose within the target tissue selectively with minimal toxicity to the surrounding normal tissue (3). And choosing an ideal clearance mechanism is one of the important factors in the design of TRT. Rapid clearance and short circulation time lead minimal background activity. Slow clearance and long circulation time allows greater accumulation in the target sites. And particle size plays a key role in clearance from the body. Small particles (<10 nm) is cleared through renal excretory system and larger particles (>10 nm) is cleared through the liver and the mononuclear-phagocyte system, which is relatively slow (4).

Small molecular type is thought to have effective targeting efficacy based on their lower molecular weight and higher permeability. Fast clearance of radiolabeled small molecules from the blood pool leads low background activity, which is beneficial. However, too rapid renal clearance during short time could be a hurdle with concerns about limitation of being taken up by the target organ after first-pass distribution and radiation exposure to the kidneys (5).

Nanoparticles conjugated with target peptide molecules generally has prolonged blood circulation time and be expected to have effective targeting efficacy because it has adequate time to reach and bind the target cell. And it has a large surface area that can be versatile by various surface modification method.

Albumin was introduced to be a suitable nanoparticle without significant side effect because it is naturally existed molecules in the human body (6). It is nontoxic, non-immunogenic and biocompatible. Human serum albumin is consists of a single chain 585 amino acid protein with a molecular weight of 66.5 kDa and escapes renal filtration due to its size above the threshold for renal clearance (7). And also, its pH-dependent interaction with the neonatal Fc receptor (FcRn) is known to have protective role from intracellular degradation (8, 9). Therefore, it has exceptionally long blood circulation time with approximate half-life of 19 days in human serum compared with other circulating proteins (7, 10, 11). Many early researchers has attracted to these properties of the albumin as a carrier for drug delivery while assuming that albumin-based nanoparticle gives an adequate time to reach target organ. Since Abraxane, a FDA-approved albumin-based nanomedicine for metastatic breast cancer, successfully proved that albumin is a clinically applicable nanoparticle, albumin gets a lot attention from many researchers (12, 13). In nuclear medicine field, albumin has been radiolabeled to be used for blood pool imaging. But in the case of high radionuclide dose for therapy, high radioactivity in blood pool might be problematic because of radiation exposure to the bone marrow.

***Voxel dosimetry with PET/CT for TRT***

Only for nuclear medicine imaging, radiation exposure to the normal tissue is not a critical radiobiological concern. However, in terms of TRT, it is always better for the absorbed dose to be determined as accurately as possible. And to know the maximum safe dose is one approach to set administered radiopharmaceutical dose.

The method called MIRD, Medical Internal Radiation Dose, has conventionally been used for estimation of absorbed doses at the organ level (14). This method assumed a homogenous distribution of radioactivity in each organ and a generalized geometry using S-value, which is mean absorbed dose in a target organ per radioactivity decay in a source organ. So, it has inherent limitation in dose estimation due to anatomical diversity and variable radioactivity distributions.

Voxel-based dosimetry using Monte Carlo (MC) simulation is considered to produce the more realistic dose distribution in the organs at the voxel-level with high precision since it reflects actual tissue heterogeneity and radioactivity distribution in the whole body (15). Therefore, to determine upper limit of injected radioactivity below normal tissue toxicity for TRT, voxel-based dosimetry is preferable.

Copper-64 ($^{64}Cu$), one of the well-known long-lived positron emitter with a half-life of 12.7 hours, has emerged as a promising radionuclide for imaging and therapy. From the physical aspect, $^{64}Cu$ has valuable characteristics that make it a multipurpose radionuclide (16, 17). It has a so complex decay scheme, which is simultaneous emission of positron and beta minus radiations that it can be used both for diagnostics and therapeutic purposes. Not only the positron emission (17.4%) without abundant gamma emission allows high resolution PET images but also beta emission (39%) allows therapeutic potentials with a high local radiation dose at the cellular level. Besides, the emission of Auger electrons, associated with the electron capture decay (43%) add the therapeutic effectiveness once the radionuclide is internalized inside the cells and located within or close to the nucleus. Therefore, $^{64}Cu$ is a promising radionuclide having a potential to be used for TRT to enable accurate dosimetry using PET imaging during therapy.

***PSMA-targeting TRT for prostate cancer***

Prostate cancer is the most frequently diagnosed male cancer in many countries (18) and 5$^{th}$ common male cancer in Korea in 2015 with constant increasing trends for the whole period from 1983 to 2015 (19). The prostate-specific membrane antigen (PSMA) is a type II membrane glycoprotein and is primarily expressed in the normal human prostate epithelium (20). Because PSMA is overexpressed in prostate cancer up to 1000 fold and is not secreted from the prostate epithelium, it was introduced as an attractive target for prostate cancer imaging and treatment (21, 22).

PSMA radiopharmaceuticals are used in a cutting-edge clinical medicine field for diagnostic imaging or therapeutic purpose (23-30). Many of the developed PSMA targeting molecules are small molecular type. Glutamate-Urea-Lysine

(GUL) derivatives is one of the PSMA targeting molecule and also commonly used as a radiolabeled molecule (31).

With the drawback of rapid blood clearance of small molecular type GUL, as mentioned earlier, albumin-based PSMA targeting nanoparticle has recently been proposed in view of therapeutic application to elongate blood circulation time and to increase radiotracer accumulation in the tumor tissue (21, 32-34). Umbricht et al. reported that PSMA ligands comprising an albumin binder, $^{177}$Lu-PSMA-ALB 56 showed better therapeutic effects on PSMA-positive tumor xenografts of mice compared with small molecular $^{177}$Lu-PSMA 617 did (32). In another report by Kuo et al., the albumin-binder-conjugated $^{177}$Lu-HTK01169 showed 3.7-fold higher peak uptake and 8.3-fold higher overall radiation dose to PSMA-positive tumor xenografts compared with $^{177}$Lu-PSMA 617 did (21).

# Purpose

The purpose of this study was to compare radiation exposure to the normal tissues between single peptide radiotracer, $^{64}Cu$-GUL and albumin-based nanoparticle radiotracer, $^{64}Cu$-albumin-GUL by biodistribution and voxel-based absorbed dose measurement using PET/CT image to simulate the maximum safety dose for their clinical application in TRT in the future.

# Materials and methods

### *Preparation of $^{64}$Cu-GUL*

NOTA-GUL kit (35) vial was purchased and added with $^{64}CuCl3$ in 0.1 M HCl solution (1.0, 2.0 or 3.0 mL). The vial was vigorously mixed for 1 min and then was incubated at room temperature for 10 min. The radiolabeling efficiency was evaluated by instant thin layer chromatography-silica gel (ITLC-SG) with 0.1 M $Na_2CO_3$ as the eluent and detected with a radio-TLC scanner.

### *Conjugation of albumin with ADIBO-NHS*

Human Albumin Fraction V was purchased from MP Biomedicals (Aurora, Ohio, USA). Azadibenzocyclooctyne-NHS ester (ADIBO-NHS) and 2,2',2''-(2-(4-(3-(3-azidopropyl)thioureido)benzyl)-1,4,7-triazonane-1,4,7-triyl)triacetic acid ($N_3$-NOTA) were purchased from FutureChem (Seoul, Korea).

The modification of albumin for conjugation of GUL and chelator on albumin surface was performed using previous method on paper and having slightly modify the procedures (36). Albumin was dissolved in phosphate buffered saline (PBS) at a concentration of 10 mg/mL. ADIBO-NHS were dissolved in DMSO (1 mg/10 μL), and then 6 uL of ADIBO-NHS was added to albumin solution. The 7.5 molar excess of ADIBO group was used to make the ADIBO functionalized albumin. The reaction vials were incubated at room temperature for two hours. Size exclusion chromatography was done using a PD-10 column with PBS as the mobile phase.

Collected albumin conjugates were examined using Nano-drop for concentration and matrix-assisted laser desorption ionization time of flight/time of flight mass spectrometry (MALDI-TOF/TOF MS) (MALDI TOF-TOF 5800 System, AB SCIEX, Framingham, MA, U.S.A) for molecular weight.

### *Preparation of albumin-GUL conjugates*

To obtain albumin-GUL conjugate, $N_3$-GUL (280 nmole, dissolved in PBS) was added to albumin-ADIBO conjugate (70 nmole/1 mL, dissolved in PBS) and incubated at 4°C for 1 h. Albumin-GUL conjugate was further purified using the PD-10 desalting column eluted with PBS.

Collected albumin-GUL conjugates were examined using Nano-drop for concentration and using MALDI TOF-TOF 5800 System (AB SCIEX, Framingham, MA, U.S.A) for molecular weight.

### *Preparation of $^{64}$Cu-albumin-GUL*

$^{64}$Cu containing vial was blow dried by a dry $N_2$ gas above the sample in a fume hood for 1h. After the vial is completely dried, 100 µl of 1M sodium acetate buffer (pH 5.3) was added to reach pH 5, followed by the addition of $N_3$-NOTA (15 nmole). The mixture was incubated at 70 ºC for 10 min on a heat block. Radiolabeling efficiency was determined using radio-instant thin layer chromatography-silica gel

(ITLC-SG) after the radiolabeling procedure with 0.1 M citric acid ($R_f$ of radiolabeled $N_3$-NOTA = 0.4-0.5; $R_f$ of free radioisotope = 0.9-1.0; $R_f$ of radiolabeled albumin conjugate = 0.0-0.1) as the mobile phases.

Finally, $^{64}Cu$ labelled, azide-functionalized chelator was conjugated with albumin-GUL.

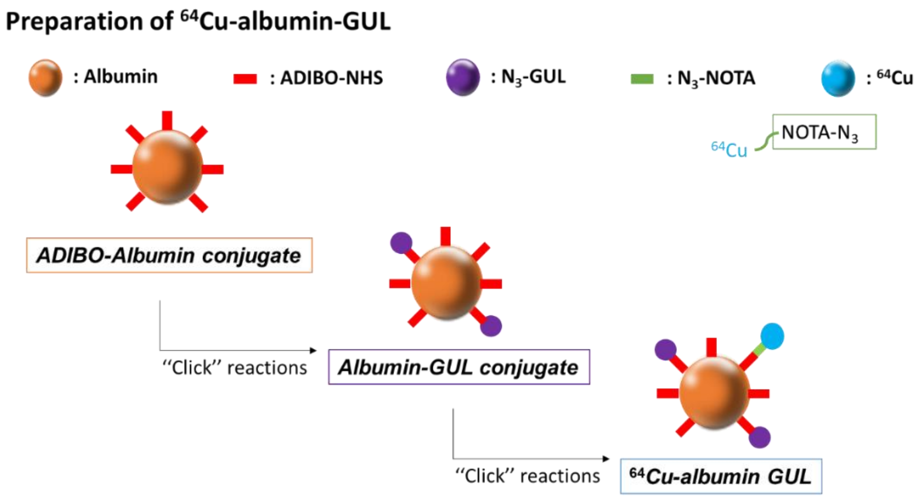


**Fugure 1. Schematics of $^{64}$Cu-albumin-GUL synthesis**

***Serum stability test***

Human serum was filtered with syringe filter, hydrophilic (0.2μm, Sartorius stedim biotech., Bohemia, NY, U.S.A). Filtered human serum was mixed with $^{64}$Cu-albumin-GUL and $^{64}$Cu-GUL were incubated 37℃ in a shaking incubator. At each time points (0.5, 1, 4, 24 and 48 h) after the probes mixed with human serum, the mixtures were analyzed using ITLC-SG with 0.1 M citric acid for $^{64}$Cu-albumin-GUL and with 0.1 M $Na_2CO_3$ for $^{64}$Cu-GUL as the solvent. The radiochemical purity was checked by radio TLC chromatogram and a percentage of value at $R_f$ = 0.0–0.1.

***In vitro competitive binding assay***

PSMA positive cell line, LNCaP cell (provided by National Cancer Center, Korea) was grown in the IMDM (Thermo Fisher Scientific, Gibco 12440-053). LNCaP cell was harvested at an 80% confluence, plated in 24 well plates at approximately 1 × $10^6$ cells/well and incubated overnight in a humidified incubator at 37 ˚C with 5% $CO_2$. $^{68}$Ga-GUL was diluted in serum-free cell culture medium containing 0.5% bovine serum albumin. Serial diluted samples each 0.5mL were added to the cells in the presence of 0.5mL cold GUL (250 μM) and incubated for 1h in a humidified incubator at 37 ˚C, 5% $CO_2$. After 1h, the medium was aspirated and the pellet was washed twice. 1mL of 1 % sodium dodecyl sulfate in phosphate buffer saline solution was added to the plates and gently mixed. The mixture was transferred to 5mL disposable plastic test tubes and their radioactivity was counted with a gammacounter. The binding curve was drawn in the excel sheet and the total estimated concentration of binding sites, Bmax and the equilibrium dissociation constant, Kd values were calculated by curve fitting.

.

***Animal PET/CT imaging***

The Institutional Animal Care and Use Committee at Seoul National University approved all animal care and experiments for this research. Specific pathogen-free 5 to 7-week-old normal male balb/c mice were used for this study. The first group of mice was injected with $^{64}$Cu-GUL and second group of mice was injected with $^{64}$Cu-albumin-GUL via tail vein injection after anesthetization by 2% isoflurane at 1.5-2 L/min oxygen flow for 5 minutes.

Dedicated small animal positron emission tomography/computed tomography (PET/CT) scanner (eXplore VISTA, GE Healthcare, WI) was used for PET imaging. Dynamic whole body PET imaging (2 beds) was started right after radiotracer injection and was acquired for 60 minutes with the energy window 250-700 keV. Those 60 minutes were consists of 5 sec/bed × 6, 30 sec/bed × 5, 90 sec/bed × 3, 150 sec/bed × 5, 10 min/bed × 2. CT scanning was followed after PET scanning was finished without moving mouse. The CT acquisition was performed for attenuation map and for anatomical information using 140 uA tube current and 40 kVp. We further acquired serial PET images at 4.5 hour and 20 hour for 5 min per bed and 48 hours for 10 min per bed after the radiotracer injection (Figure 2).

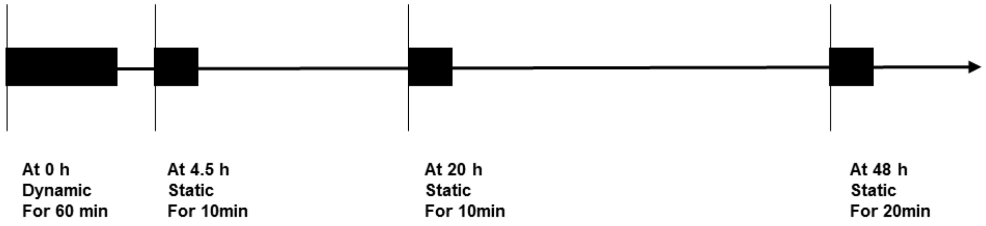


**Figure 2. Scheme of animal experiment of PET imaging**

This is schematic diagram of animal experiment of PET imaging. Dynamic images of mouse (2beds) were acquired for initial 60 minutes, consists of 5 sec/bed $\times$ 6, 30 sec/bed $\times$ 5, 90 sec/bed $\times$ 3, 150 sec/bed $\times$ 5, 10 min/bed $\times$ 2. Static images of mouse (2beds) were followed with acquisition for 5min per bed at 4.5 h and 20h, and for 10 min per bed at 48h.

***Urine analysis***

When acquisition of the initial 1hr dynamic PET/CT images finished, urines of the mice in each group were examined by a radio-TLC scanner. Urine of mouse with $^{64}$Cu-GUL injection was evaluated by ITLC-SG with 0.1 M $Na_2CO_3$ and urine of mouse with $^{64}$Cu-albumin-GUL injection was evaluated by ITLC-SG with 0.1 M citric acid.

***Phantom PET/CT imaging***

Uniform phantom was prepared using 50mL disposable plastic tube containing $^{64}$Cu. The volume of phantom was 58.7mL and the concentration of activity was 6.9 $\times\ 10^4$ Bq/mL the same PET/CT machine, mentioned above was used for 1hr static PET/CT image (1bed) of the phantom. CT scanning was followed after PET scanning was finished without moving it, with the same CT current and voltage parameters.

***Image reconstruction***

The PET data were reconstructed using a two-dimensional ordered-subsets expectation maximum (OSEM) algorithm with attenuation correction using CT, random correction and scatter correction was used for PET image reconstruction. The reconstructed PET images had the matrix size of $175 \times 175 \times 61$ and voxel size of $0.3875 \times 0.3875 \times 0.775$ mm$^3$.

The CT data were reconstructed using FeldKamp algorithm with a matrix size of

*1018* $\times$ *1018* $\times$ *872* and voxel size of *0.06* $\times$ *0.06* $\times$ *0.06* $mm^3$.

The CT and PET DICOM images were post processed using AMIDE tool to match the voxel size of 0.39 $\times$ 0.39 $\times$ 0.39 $mm^3$ for MC simulation. The voxel intensity of PET images was given in the standardized uptake value (SUV).

***Measurement of correction factor***

The volume of interest (VOI) was drawn over the reconstructed uniform phantom image and mean SUV of VOI) was measured, which was corrected to Bq/cc. Correction factor for the conversion of calculating activity concentration from SUV (PET image) into actual activity concentration was calculated by dividing the initial activity concentration (Bq/cc) in the phantom to the measured activity concentration (Bq/cc).

***PET image-based biodistribution***

VOIs were manually drawn over the major organs of the mice (brain, heart, lungs, liver, and kidneys), slice by slice on CT images at different time points with the help of the co-registered CT and PET images. Mean SUVs obtained by VOIs of the organs were converted into actual activity concentration (Bq/cc) with the help of correction factor. The activity of each organ (Bq) was normalized to the total injected dose (%ID) of each radiotracers and the total injected dose (%ID) vs. time curves and the total injected dose per gram (%ID/gm) were presented. The cumulated activity (MBq.hr) in each organ was calculated by the trapezoidal summation of the area under curve (AUC) of time activity curve. The residence time was calculated from the formula of cumulated activity divided by injected activity of $^{64}$Cu-GUL or $^{64}$Cu-albumin-GUL in each mouse.

### *GATE Monte Carlo simulation*

GATE v.7.0, has been used for simulations to calculate absorbed dose in this study (37). GATE which has been extended for dosimetry simulations is based on the Geant4 toolkit, a well-established code for radiation transport (38). This version of GATE makes use of Geant4 v. 9.6.3. The size of PET and CT images of mice were resampled to match the voxel dimensions (*0.3875* mm × *0.3875* mm × *0.775* mm). The CT image (attenuation map) and the PET image (activity distribution map) were used as voxelized phantom and voxelized source respectively as the inputs for GATE simulation. ImageRegularParametrisedVolume option of GATE was chosen for voxelized phantom using mouse CT image and $^{18}$F ion source type of Geant4 v. 9.6.3 was used for all simulations in this study. Standard electromagnetic physics package of GATE MC, which includes photoelectric effect, Compton, bremsstrahlung and positron-electron annihilation, was used during all simulations. GATE was run with Mersenne Twister (39) random number generator where the energy cuts and variance reduction techniques were not applied in the physical processes. The simulation was conducted in an in-house computing cluster with a 60-core CPU and 80 GB of RAM to reduce the simulation time. A separate simulation for each PET frame was performed with the corresponding biodistribution and PET frame duration. During each simulation, the statistical uncertainties were kept below 2% at the voxel-level.

***Voxel-based absorbed dose calculations using GATE MC (40)***

The outputs of the GATE simulations are the energy deposition (Edep) map, dose distribution map (dosemaps), the number of hits and the local statistical uncertainty. GATE MC contains a mechanism, named DoseActor, which stores the absorbed dose in a given volume in a 3D matrix (41). The deposited energy [J] in each voxel was extracted using DoseActor mechanism from all the Dose maps with the help of VOIs previously drawn on CT and PET images. The absorbed dose in a voxel was subsequently calculated by dividing the voxel energy with the voxel mass obtained in this study. The absorbed dose in the organ was finally calculated by summing all the voxel doses with that organ. We then calculated dose rates (Gy/hr) in the organs from each PET frame by dividing the absorbed dose with the respective simulation time. The dose rate vs. time curves were plotted to measure the total absorbed dose in each organ using AUCs. The estimated absorbed dose at voxel-level was normalized to the injected activity of $^{64}$Cu-GUL or $^{64}$Cu-albumin-GUL in each mouse and presented as mGy/MBq.

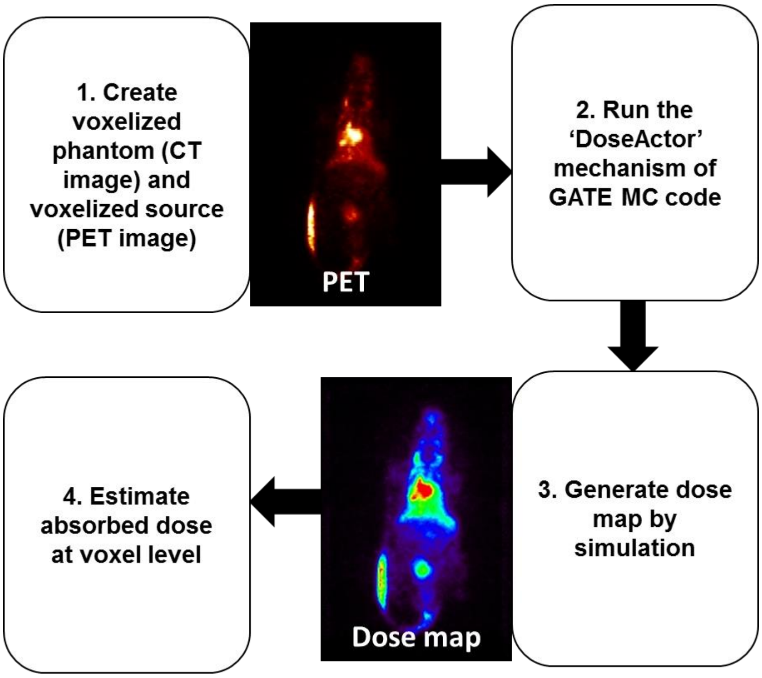


**Figure 3. Schematics of GATE MC simulation for absorbed dose estimation at voxel level**

# Results

### *Radiolabeling of NOTA-GUL and albumin-GUL using click chemistry*

Radiolabeling was performed immediately before the scheduled experiments considering half-lives of radioisotopes. Labeling efficiencies of $^{64}Cu$ with NOTA-GUL or albumin-GUL were measured by radio-TLC scanner and they both were over 95% (Figure 4).

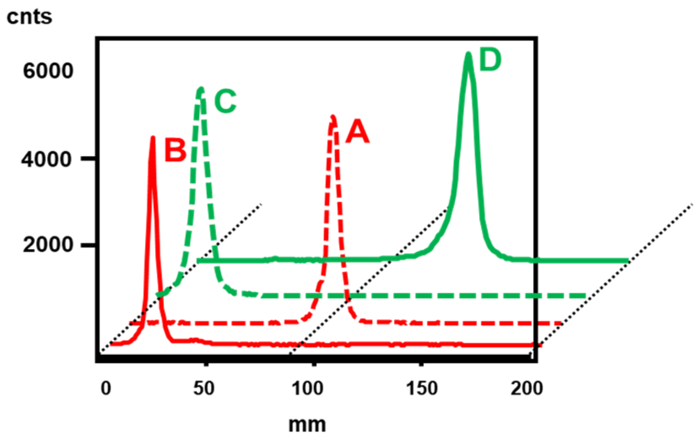


(A) Red dotted line: Free $^{64}Cu$ eluted with Citric acid
(B) Red line: $^{64}Cu$-albumin-GUL eluted with Citric acid
(C) Green dotted line: Free $^{64}Cu$ eluted with 0.1 M $Na_2CO_3$
(D) Green line: $^{64}Cu$-NOTA-GUL eluted with 0.1 M $Na_2CO_3$

**Figure 4. Radiolabeling efficiencies of $^{64}Cu$-GUL and $^{64}Cu$-albumin-GUL**

Radiolabeling efficiencies of $^{64}Cu$ with NOTA-GUL or albumin-GUL were over 95%.

### *Determination of the conjugation number*

Molecular weights of the collected ADIBO-albumin and albumin-GUL were measured by MALDI TOF/TOF MS to estimate the number of attached ADIBO-NHS and GUL moieties on albumin. Molecular weights of the albumin, ADIBO-albumin and albumin-GUL were 66475, 68980 and 70164, respectively. The estimated number of ADIBO conjugation was about 7, which is considered as degree of functionalization (DOF). Number of GUL attached on the albumin was calculated to be about 2 (Figure 5).

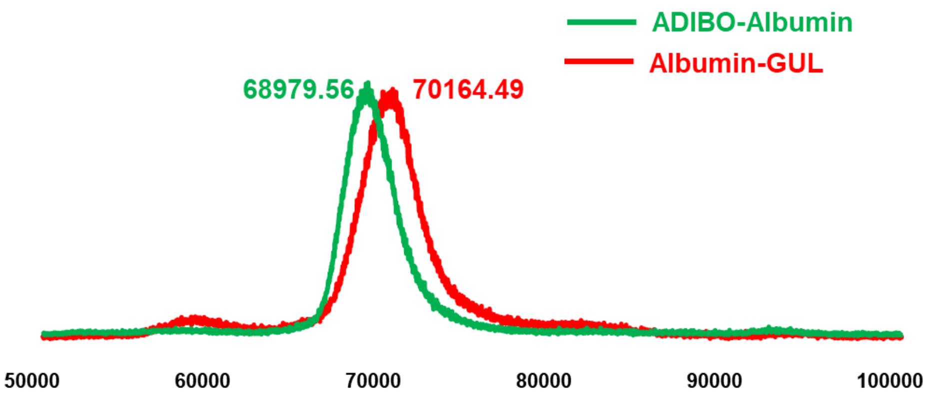


| Type | Molecular weight (mean) | Conjugation No. on the albumin | Remarks |
|---|---|---|---|
| Albumin | 66475.1 | 0.00 | Control |
| ADIBO-Albumin (a) | 68979.56 | 6.96 | Degree of functinaliztion |
| Albumin-GUL (b) | 70164.49 | (b)-(a)/548.54 = 2.16 | Exact mass: 548.54 g/mol |

**Figure 5. Determination of the conjugation number**

The estimated number of ADIBO conjugation was about 7, which is considered as degree of functionalization. The number of GUL attached on the albumin was calculated and it was about 2.

### *Serum stability test*

The radiochemical purities of both radiotracers, checked by radio TLC chromatogram, were over 95% up to 48 h (Figure 6).

(A)

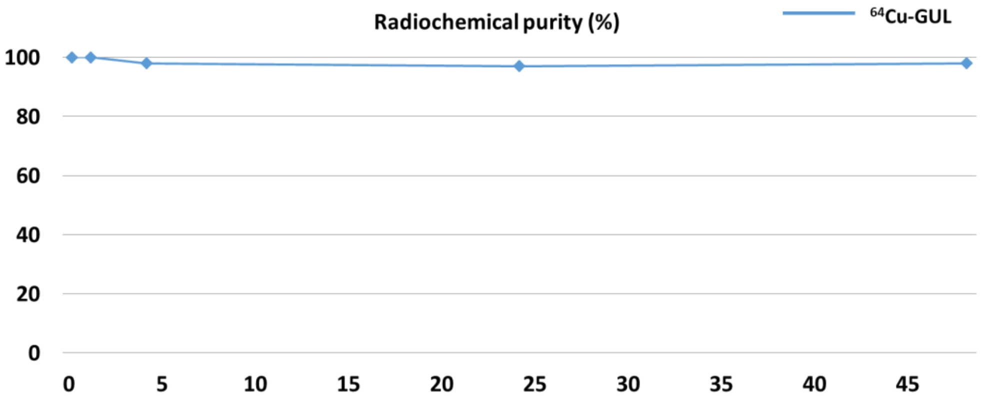


(B)

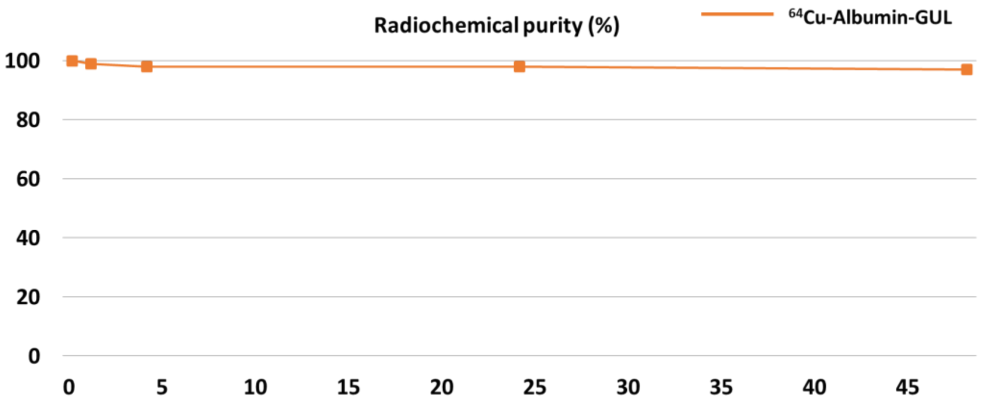


**Figure 6. Serum stability test**

The radiochemical purities of both radiotracers were over 95% up to 48 h.

### *In vitro affinity test*

Bmax and Kd values were calculated through in vitro competitive binding assay. As the concentration of $^{64}$Cu-GUL was increased, the radioactivity of LNCaP was increased in the presence of another PSMA binding small molecule, which means PSMA-specific binding of $^{64}$Cu-GUL was increased. Bmax and Kd values were 0.0672 and $9.337 \times 10^{-9}$, respectively (Figure 7).

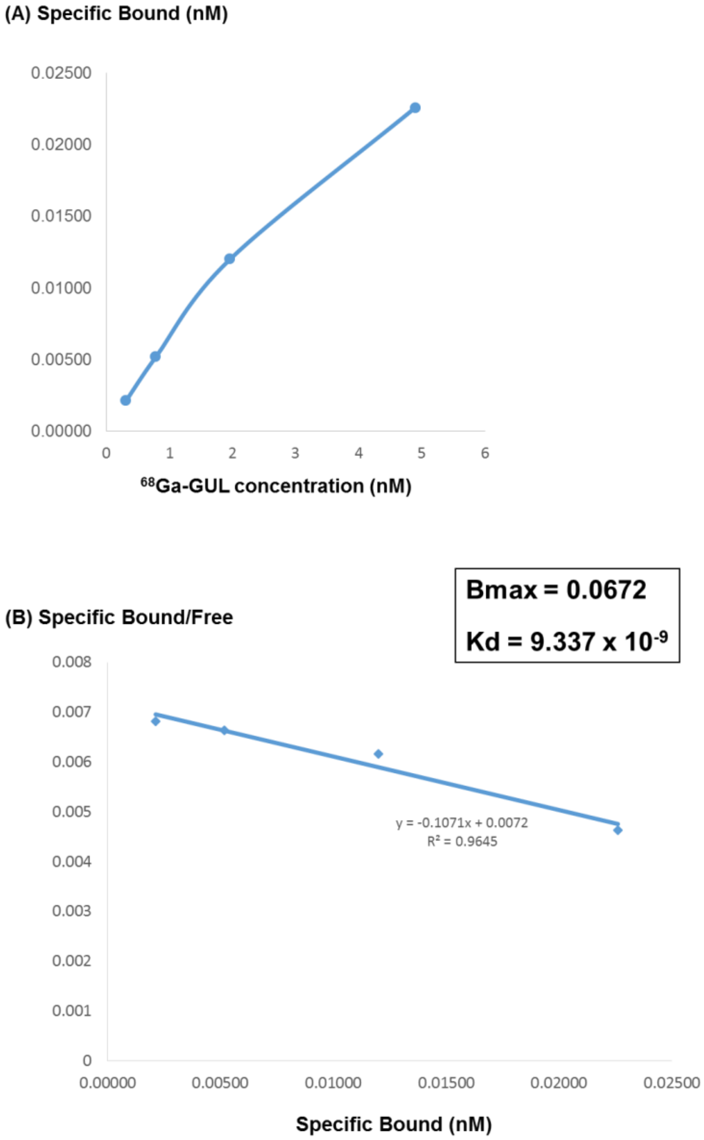


**Figure 7. *In vitro* affinity test**

(A) PSMA-specific binding of $^{64}$Cu-GUL was increased as the concentration of $^{64}$Cu-GUL was increased in the presence of PSMA inhibitor.

(B) Bmax and Kd values, calculated through in vitro competitive binding assay, were 0.0672 and $9.337 \times 10^{-9}$, respectively.

### *In vivo animal study*

Serial PET images were obtained after tail vein injection of $^{64}$Cu-GUL and $^{64}$Cu-albumin-GUL using a dedicated animal PET/CT scanner. Maximum intensity projection PET images after $^{64}$Cu-GUL and $^{64}$Cu-albumin-GUL injection via tail vein were demonstrated (Figure 8, 9). The initial dynamic images for 60 minutes were reconstructed into 21 frame images (Figure 8B, 9B). Static PET images were obtained for 5 minute per bed for 2bed at 4.5 h and 20 h and for 10 minute per bed for 2bed at 48 h.

Accumulation of $^{64}$Cu-GUL was noted dominantly in the kidneys and then bladder sequentially within 60 minutes, which means early urinary excretion. Accumulation of $^{64}$Cu-albumin-GUL is noted mainly in the blood inside the heart and in the liver, and this distribution persists after 60 minute. Minimal radioactivity is noted in the bladder.

**(A)**

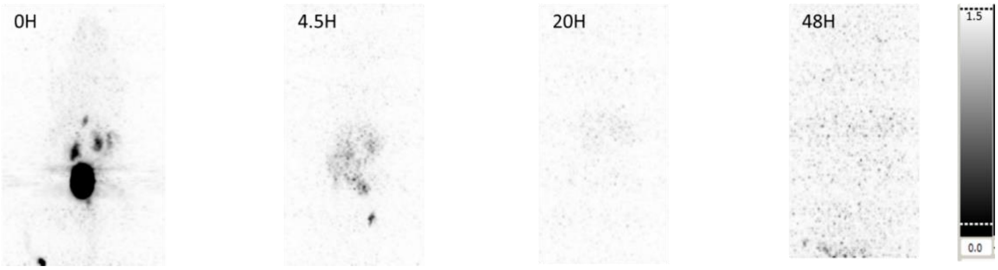


**(B)**

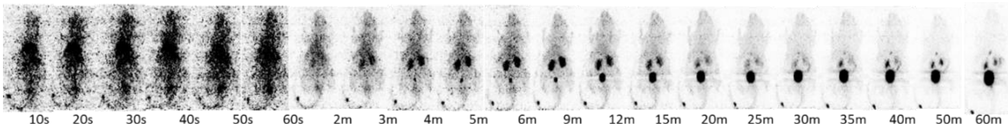


**Figure 8. *In vivo* PET results of $^{64}$Cu-GUL**

(A) Maximum intensity projection PET images after $^{64}$Cu-GUL injection via tail vein up to 48 h were demonstrated. The 1st image is the summation images during 0~60 minutes.

(B) Maximum intensity projection PET images of 21 frames during the initial 60 minute dynamic study were demonstrated. Accumulation of $^{64}$Cu-GUL is dominantly in the kidneys and then bladder within 60 minutes due to urinary excretion.

**(A)**

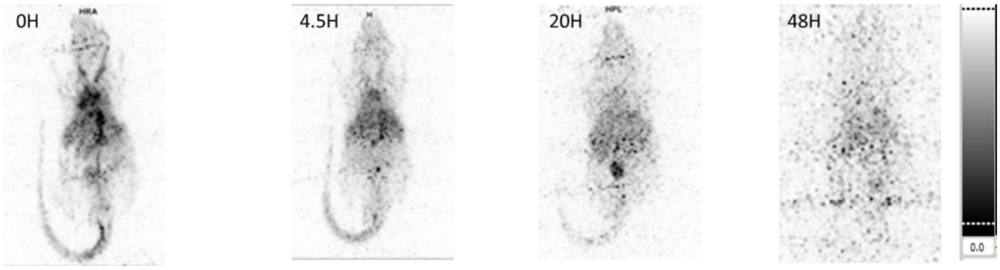


**(B)**

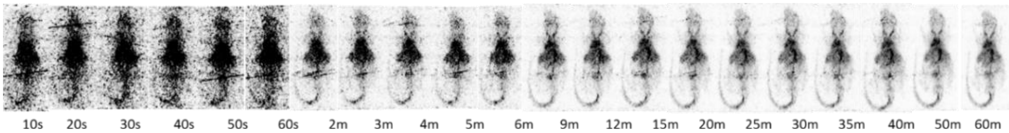


**Figure 9.** ***In vivo*** **PET results of $^{64}$Cu-albumin-GUL**

(A) Maximum intensity projection PET images after $^{64}$Cu-albumin-GUL injection via tail vein up to 48 h were demonstrated. The 1st image is the summation images during 0~60 minutes.

(B) Maximum intensity projection PET images of 21 frames during the initial 60 minute dynamic study were demonstrated. Radioacitivity of $^{64}$Cu-albumin-GUL is mainly localized in the blood inside the heart and in the liver. This distribution lasts after 60 minute.

***Urine analysis***

Urine TLC results of the mouse after 1hr $^{64}Cu$-GUL injection shows almost identical peak with that of the $^{64}Cu$-GUL (Figure 10). However, urine TLC results of the mouse after 1hr $^{64}Cu$-albumin-GUL injection shows minimal peak at the location of the free $^{64}Cu$ (Figure 11).

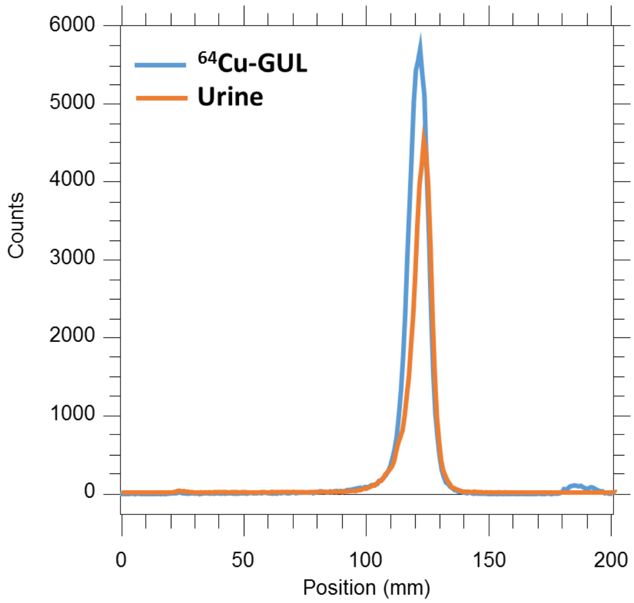


**Figure 10. Urine TLC results after 1 hr of $^{64}$Cu-GUL injection**

Urine of the mouse with $^{64}$Cu-GUL injection was examined by ITLC-SG with 0.1 M $Na_2CO_3$ after acquisition of the initial 1hr dynamic PET/CT images. Urine TLC result shows almost identical peak with that of the $^{64}$Cu-GUL.

**(A)**

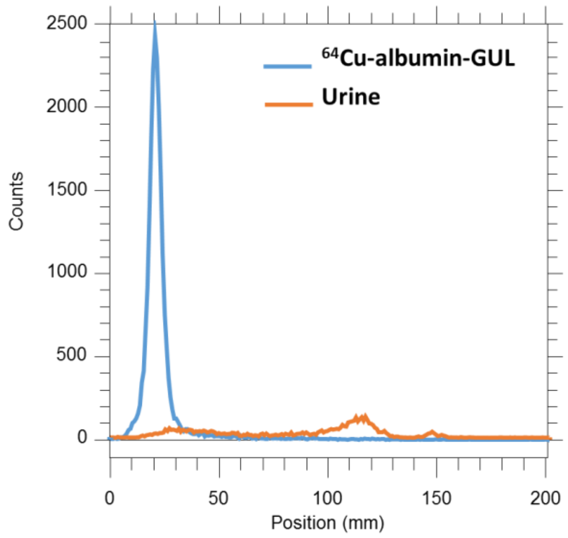


**(B)**

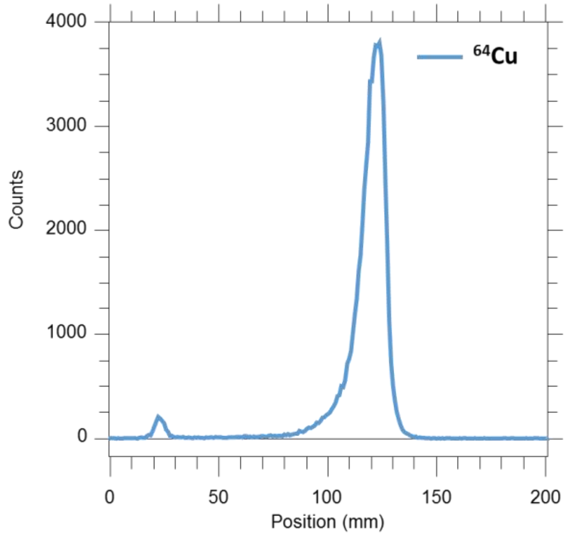


**Figure 11. Urine TLC after 1 hr of $^{64}$Cu-albumin-GUL injection**

Urine of the mouse with $^{64}$Cu-GUL injection was examined by ITLC-SG with 0.1 M citric acid after acquisition of the initial 1hr dynamic PET/CT images. Urine TLC result shows minimal peak at the location of the free $^{64}$Cu.

### *PET image-based biodistribution*

For quantification, the reconstructed uniform $^{64}Cu$ phantom image in that the activity was already known was used to calculate the correction factor for $^{64}Cu$ and it was 4.28. The reconstructed voxel intensity of PET images obtained from our PET/CT system was given in SUV. The SUVs are converted into activity using correction factor.

TACs of the brain, blood, lungs, liver and kidneys were obtained (Figure 12-14). Blood activity was calculated from the blood activity in the heart, multiplied by 1.4.

Activity of $^{64}Cu$-GUL in the kidneys was increased until 10 minute and then decreased rapidly. Other than that, the peaks of $^{64}Cu$-GUL in the brain, blood, lungs, were found within 1 minute and steadily decreased. The peaks of $^{64}Cu$-albumin-GUL in all of the major organs were also found within 1 minute, but led to the plateaus unlike $^{64}Cu$-GUL. Activity of $^{64}Cu$-albumin-GUL only in the liver slightly increased again at the 4.5 h.

The cumulated activities and residence times in the brain, heart wall, blood in the heart, lungs, liver and kidneys were described in the table 1 and Figure 15. All organs of the mouse treated with $^{64}Cu$-albumin-GUL had higher cumulated activity than that of the mouse treated with $^{64}Cu$-GUL. Liver showed the highest accumulation of radioactivity in both groups. The next highest accumulation of radioactivity was found in the lungs of the mouse treated with $^{64}Cu$-albumin-GUL and in the kidneys of the mouse treated with $^{64}Cu$-GUL.

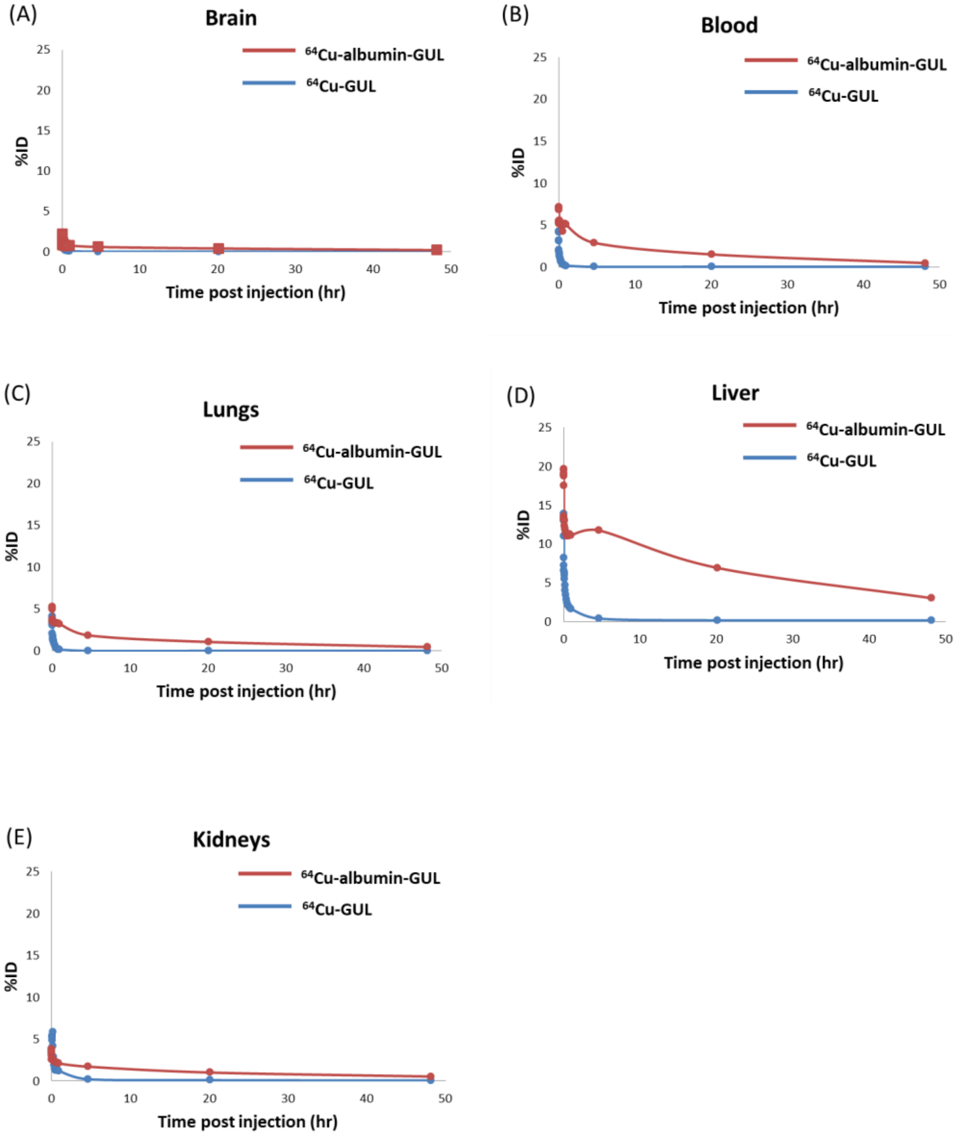


**Figure 12. Biodistribution per organ (%ID)**

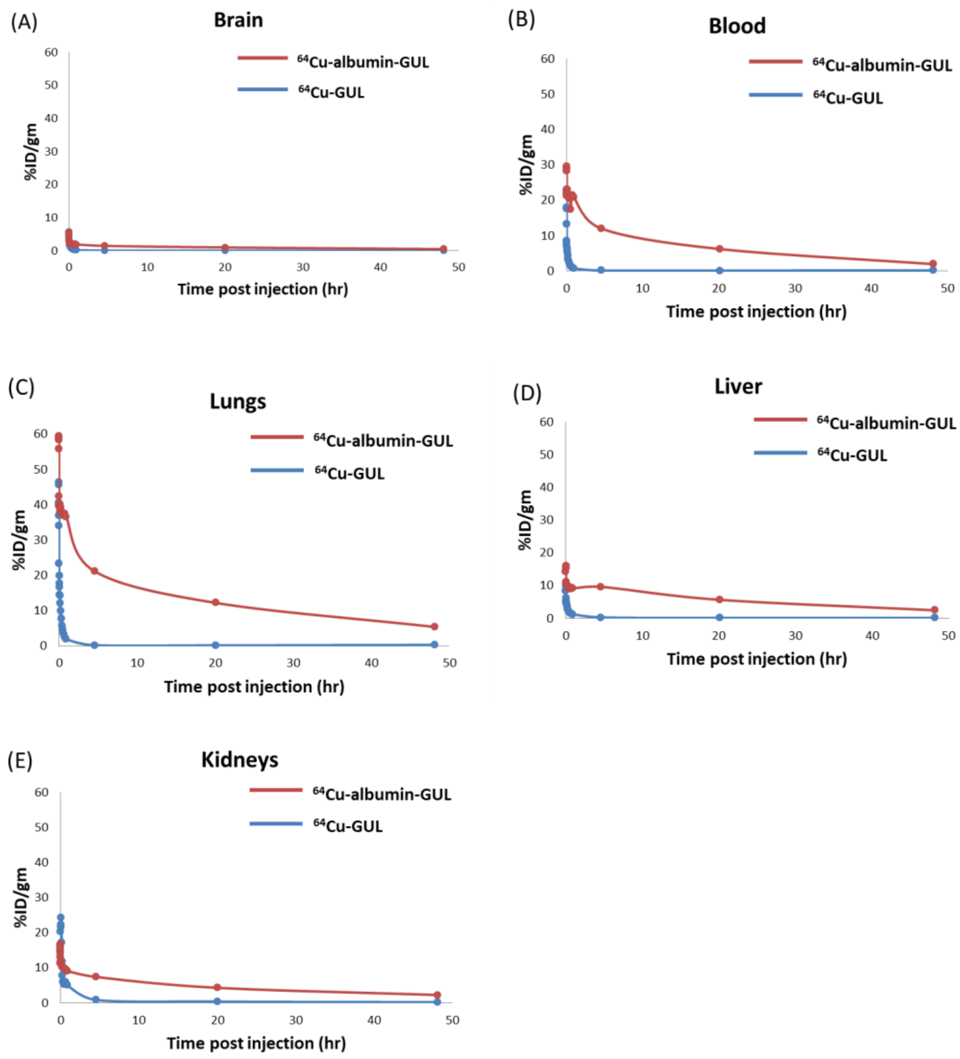


**Figure 13. Biodistribution (%ID/gm)**

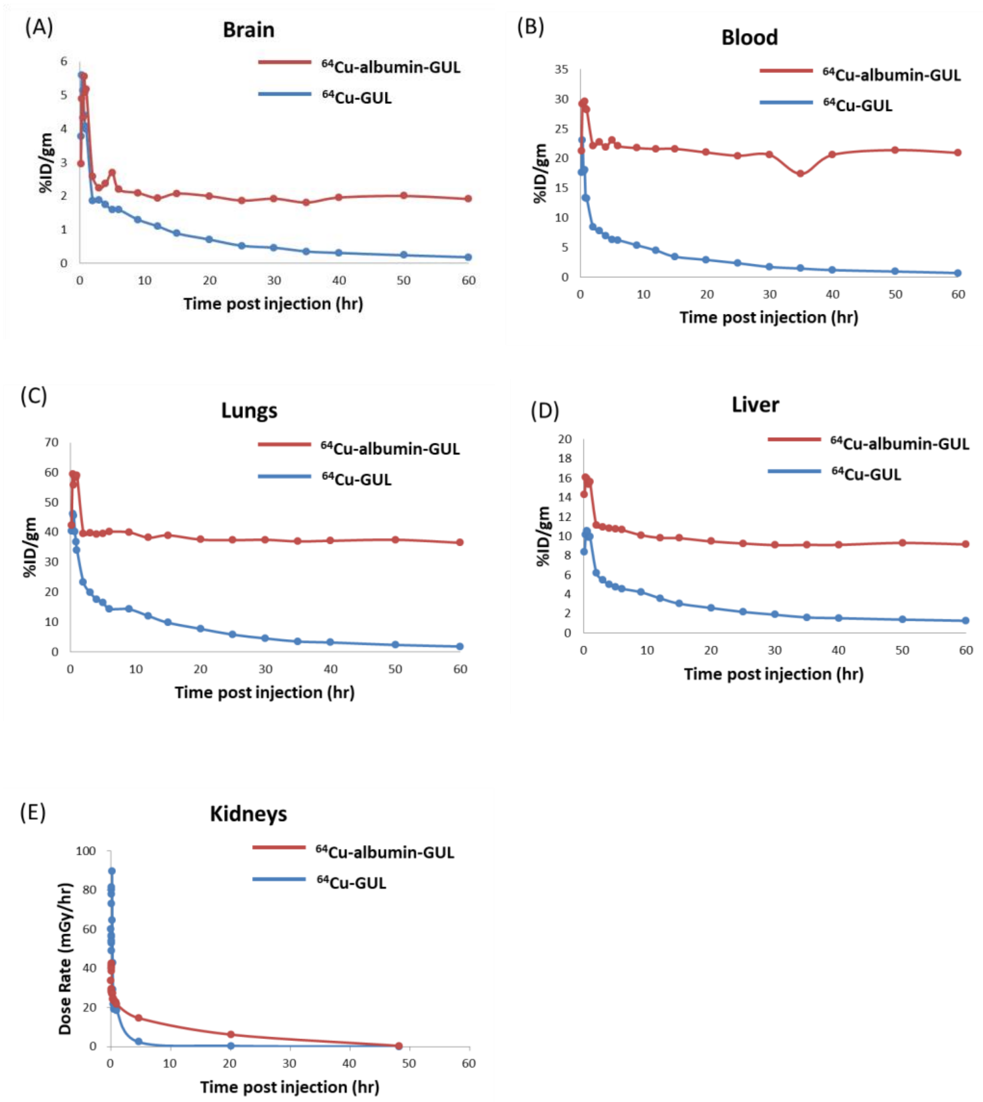


**Figure 14. Biodistribution (%ID/gm) in the initial 60 minutes**

**Table 1. Residence time (min) in the major organs**

| organ | $^{64}$Cu-GUL | | | $^{64}$Cu-albumin-GUL | | |
|---|---|---|---|---|---|---|
| | Mouse 1 | Mouse 2 | **Mean** | Mouse 1 | Mouse 2 | **Mean** |
| **Brain** | 0.33 | 0.38 | 0.36 | 6.41 | 5.53 | 5.97 |
| **Heart wall** | 0.14 | 0.10 | 0.12 | 4.06 | 3.94 | 4.00 |
| **Blood in Heart** | 0.50 | 0.40 | 0.45 | 20.1 | 20.0 | 20.0 |
| **Lungs** | 0.64 | 0.79 | 0.71 | 18.3 | 19.8 | 19.1 |
| **Liver** | 6.95 | 5.34 | 6.14 | 98.0 | 112 | 105 |
| **Kidneys** | 2.65 | 4.76 | 3.70 | 17.3 | 14.7 | 16.0 |

(A)

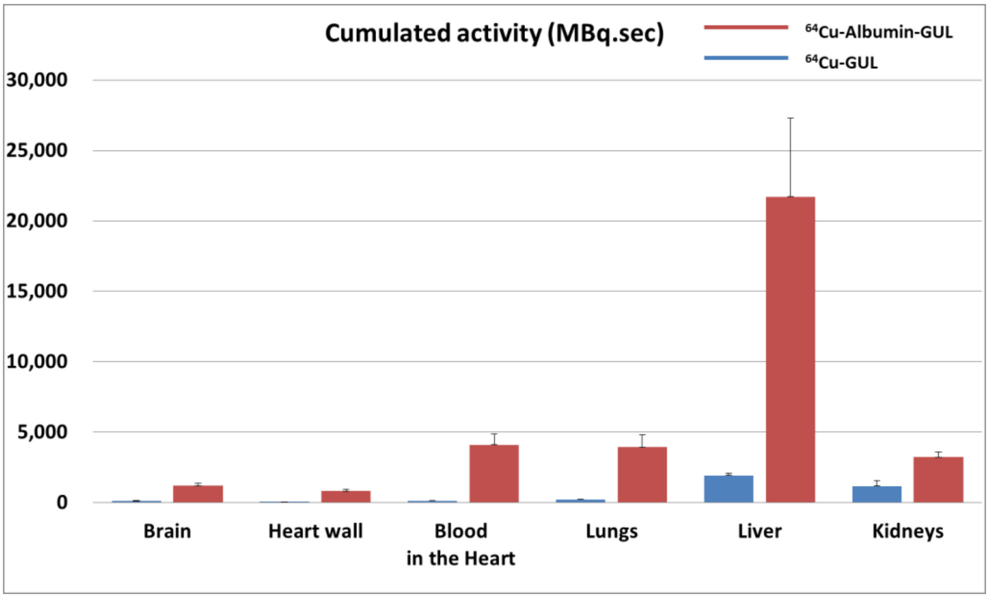


(B)

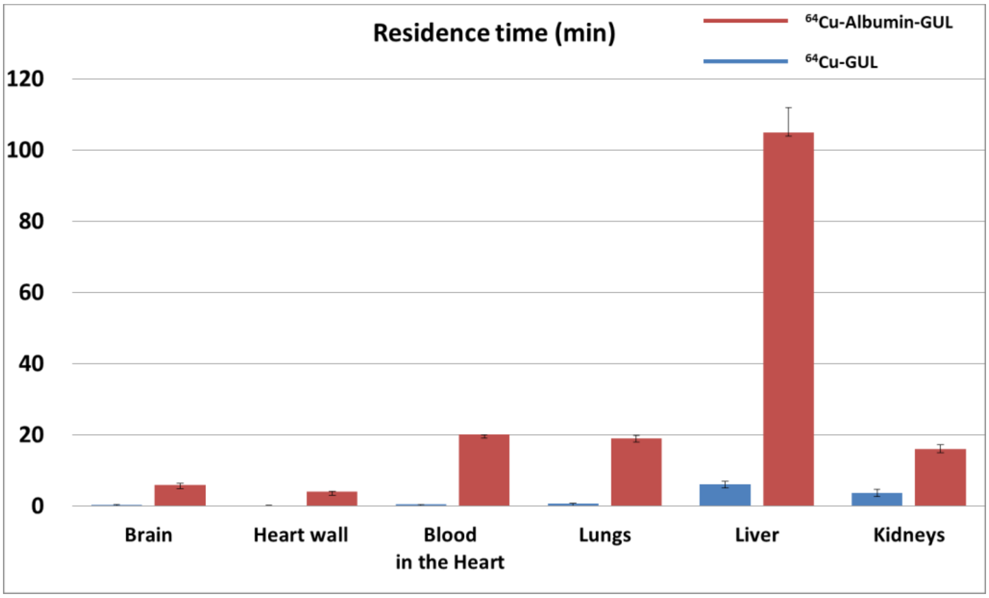


**Figure 15. Cumulated activity (MBq.sec) (A) and residence time (min) (B)**

### *Voxel-based absorbed dose*

Dose maps were simulated by GATE MC simulation method (Figure 16). Dose-rate vs. time graphs of the brain, heart wall, lungs, liver and kidneys were demonstrated in figure 17. Normalized dose rates (mGy/MBq.hr) that is expressed as dose rate per unit radioactivity of the administered radiotracer were plotted in figure 18 and 19.

The voxel-based absorbed doses (mGy/MBq) of the 5 organs in the mouse with $^{64}$Cu-GUL or $^{64}$Cu-albumin-GUL injection are presented in the table 2 with voxel size of each VOIs (n). The graphs of those were drawn and compared between groups and within the each group (Figure 20, 21 and 22).

All major organs of the mouse that treated with $^{64}$Cu-albumin-GUL had higher absorbed doses than those of the mouse that treated with $^{64}$Cu-GUL. Overall, the absorbed dose of the liver due to $^{64}$Cu-albumin-GUL was the highest (134.25 ± 22.39 mGy/MBq). In the mouse with $^{64}$Cu-GUL injection, kidneys had the highest absorbed dose. However, absorbed dose of the kidneys due to $^{64}$Cu-albumin-GUL was still higher (18.52 ± 6.48 vs. 106.63 ± 29.75 mGy/MBq, respectively).

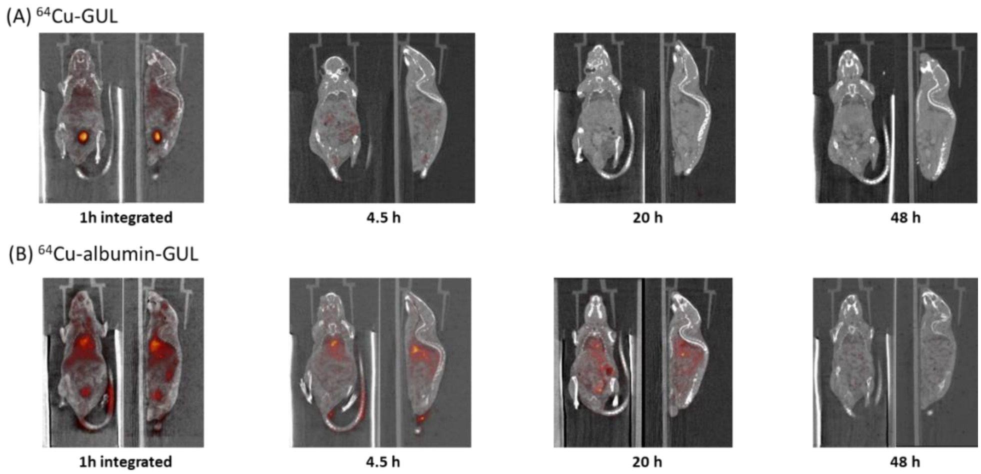


**Figure 16. Representative images of the dose maps (Gy/voxel) by GATE Monte Carlo Simulation**

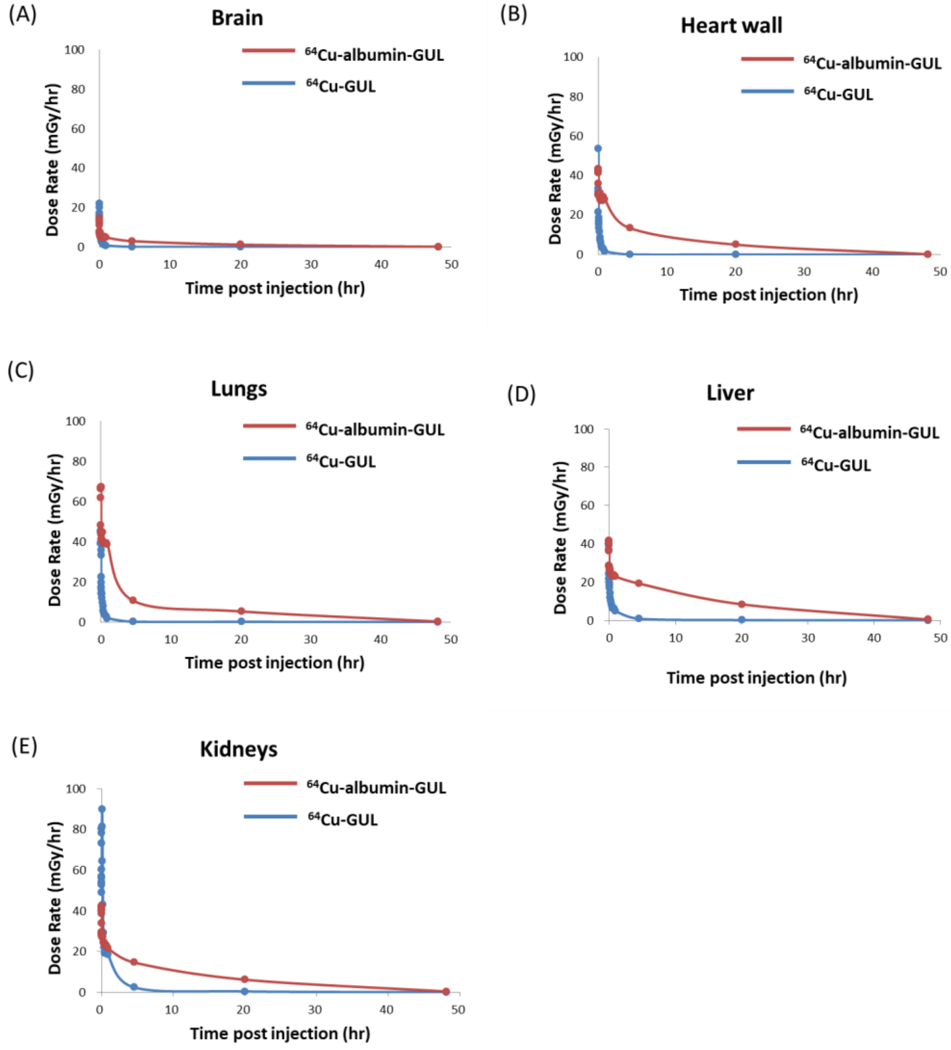


**Figure 17. Dose rate per organ (Gy/hr)**

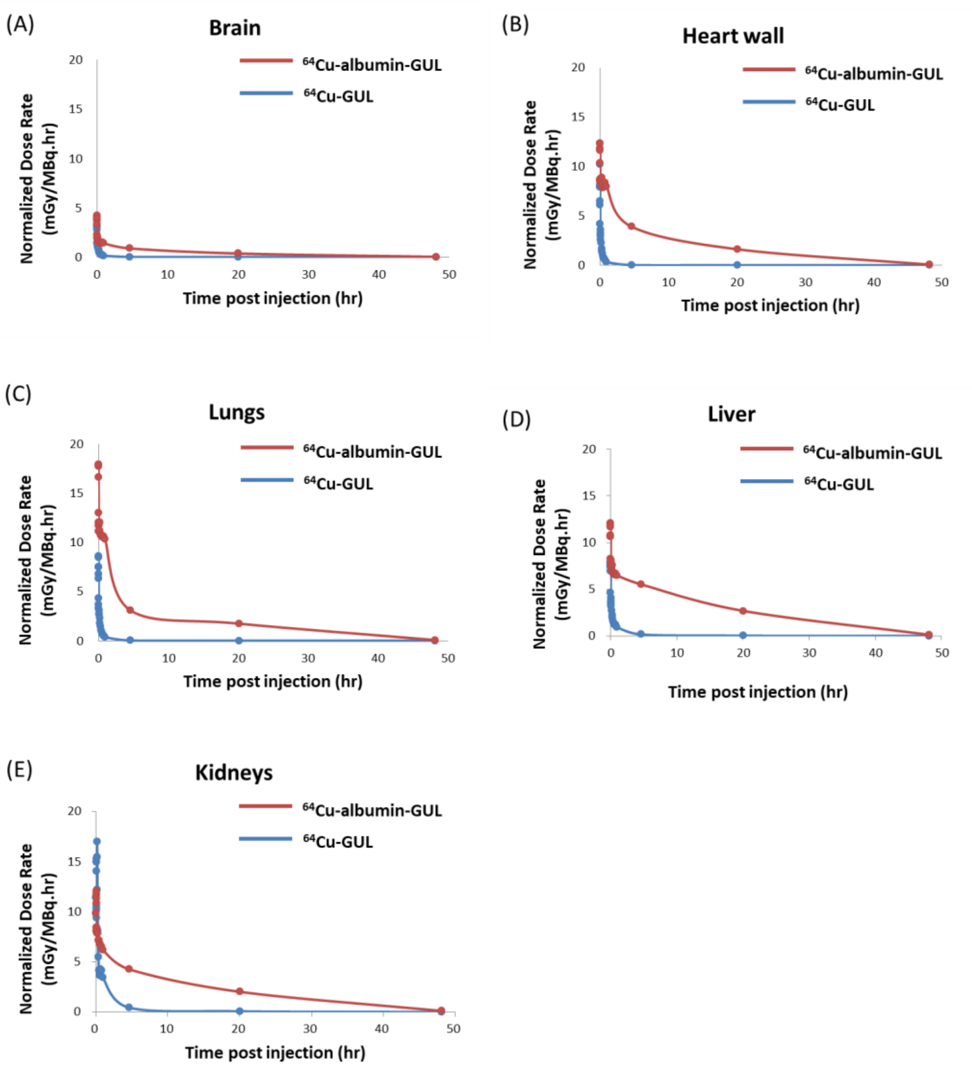


**Figure 18. Normalized dose rates (mGy/MBq.hr), expressed as dose rate per unit radioactivity of the administered radiotacers**

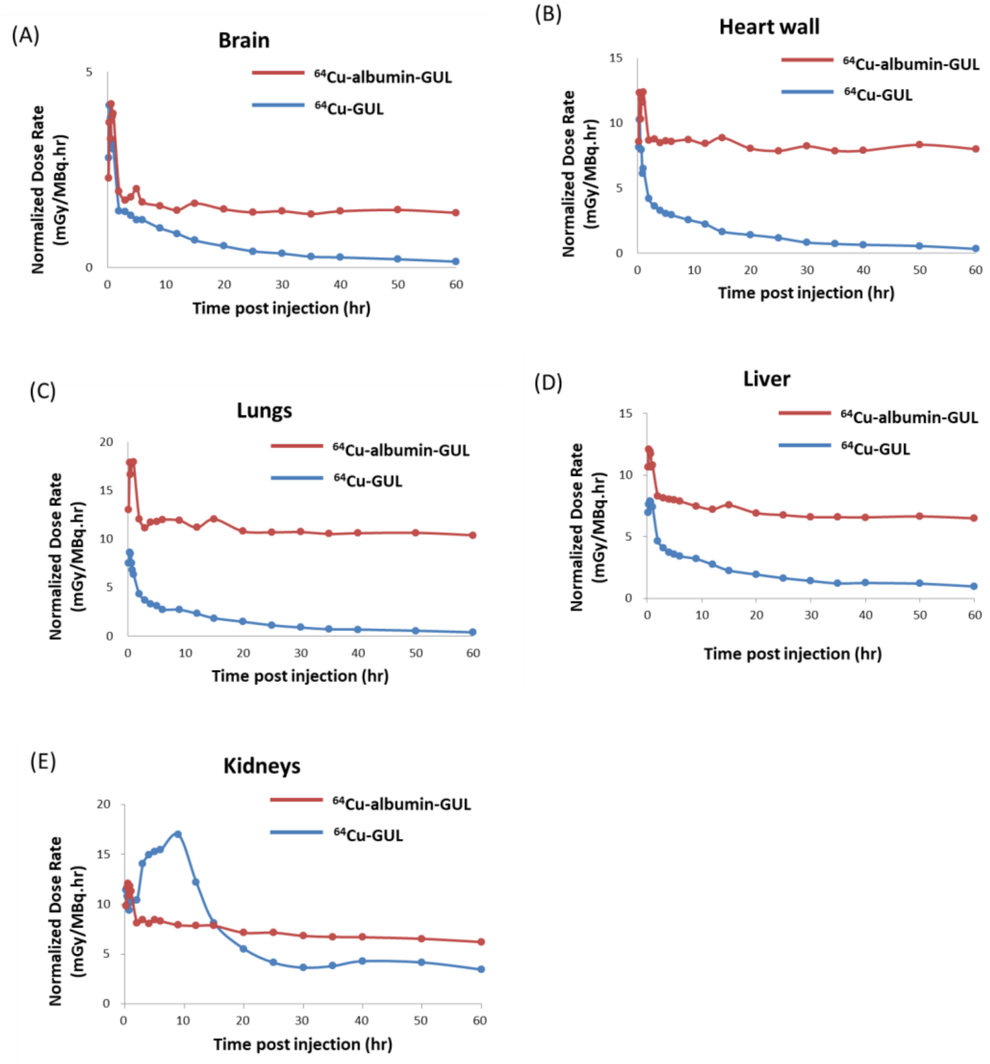


**Figure 19. Normalized dose rates (mGy/MBq.hr) in initial 60 minutes**

**Table 2. Voxel-based absorbed dose (mGy/MBq) in the major organs**

| organ | | $^{64}$Cu-GUL | | | $^{64}$Cu-albumin-GUL | | |
|---|---|---|---|---|---|---|---|
| | | Mouse 1 | Mouse 2 | **Mean** | Mouse 1 | Mouse 2 | **Mean** |
| **Brain** | absorbed dose | 1.09 | 1.43 | **1.26** | 23.72 | 18.9 | **21.33** |
| | voxel size of VOI | 6760 | 6034 | | 6871 | 6195 | |
| **Heart wall** | absorbed dose | 2.69 | 2.24 | **2.46** | 108.99 | 85.9 | **97.42** |
| | voxel size of VOI | 1101 | 1060 | | 1078 | 930 | |
| **Lungs** | absorbed dose | 2.41 | 3.08 | **2.74** | 106.57 | 92.1 | **99.34** |
| | voxel size of VOI | 5860 | 5804 | | 5789 | 5753 | |
| **Liver** | absorbed dose | 6.83 | 5.9 | **6.36** | 150.2 | 116.8 | **133.48** |
| | voxel size of VOI | 21878 | 20312 | | 20420 | 18591 | |
| **Kidneys** | absorbed dose | 13.22 | 21.69 | **17.46** | 128.99 | 85.72 | **107.35** |
| | voxel size of VOI | 3810 | 3919 | | 3966 | 3425 | |

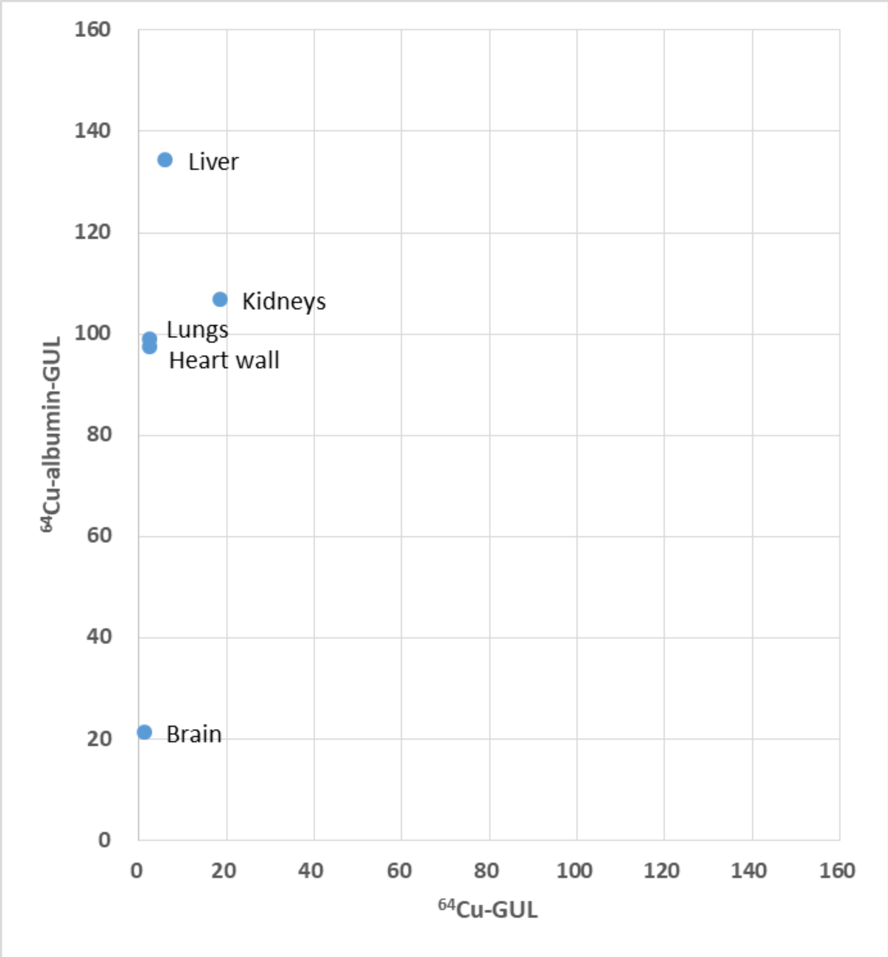


**Figure 20. Comparison of voxel-based absorbed dose (mGy/MBq) in major organs between two groups**

All major organs of the mice with $^{64}$Cu-albumin-GUL injection had higher absorbed doses than those of the mice with $^{64}$Cu-GUL injection. Overall, the absorbed dose of the liver due to $^{64}$Cu-albumin-GUL was the highest.

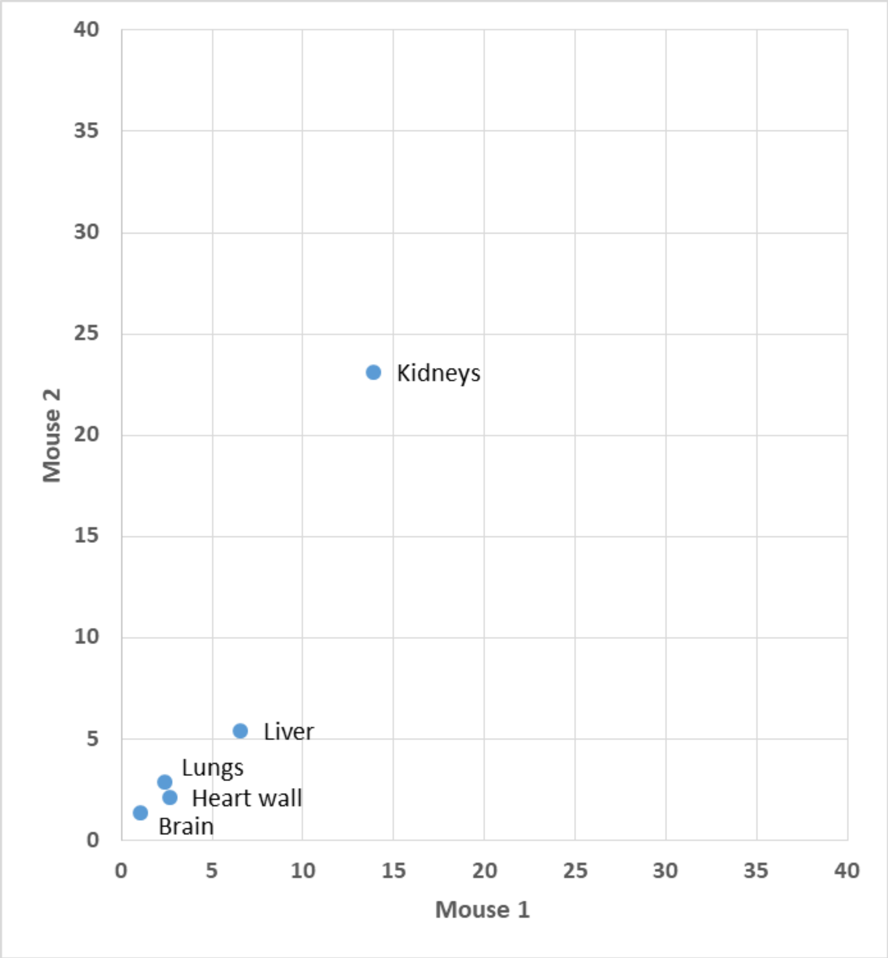


**Figure 21. Comparison of voxel-based absorbed dose (mGy/MBq) in major organs within the group of $^{64}$Cu-GUL injection**

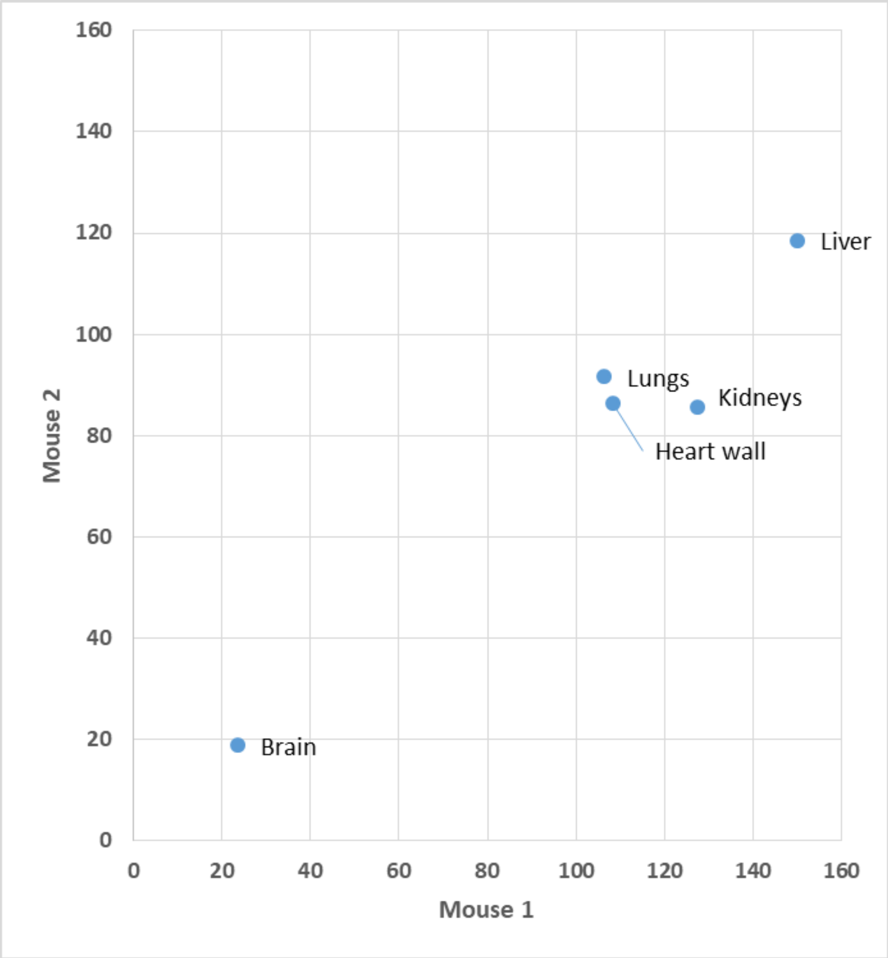


**Figure 22. Comparison of voxel-based absorbed dose (mGy/MBq) in major organs within the group of $^{64}$Cu-albumin-GUL injection**

## Discussion

Absorbed dose of $^{64}$Cu-GUL and $^{64}$Cu-albumin-GUL were compared in mice to estimate radiation exposure to normal tissue. In the results, all of the brain, blood or heart wall, lungs, liver and kidneys show higher residence time and absorbed dose when treated with $^{64}$Cu-albumin-GUL. The most important strategy for successful TRT is to deliver lethal dose to the tumor without unduly affecting healthy tissue. Because of the variable PSMA expression of the individual's prostate tumor cell, it is better for radiopharmaceutical dose to be selected as high as possible. But in any case, it should be under the maximum safety dose. Therefore, foreknowing safety dose is important.

In this study, voxel-based dosimetry using MC simulation was used to calculate absorbed dose. Till now, very few preclinical voxel-based dosimetry studies of real mouse PET images have been reported, especially using $^{64}$Cu (42). T Xie et al. reported that cross-absorbed S-value of $^{64}$Cu is the smallest among positron emitters ($^{11}$C, $^{13}$N, $^{15}$O, $^{18}$F, $^{68}$Ga, $^{86}$Y and $^{124}$I) and is significantly lower to the non-adjacent target organs (43). Because of complex decay scheme of $^{64}$Cu, different types of radiation contribute to the S-values. Photons and x-rays, electron and positron contribute to the total cross-absorbed S-value for $^{64}$Cu. While contribution of positrons to the total self-absorbed S-value is over 92% for $^{18}$F, it is less than 40% for $^{64}$Cu. Instead, electron contributes more than 50% to the self-absorbed S value for $^{64}$Cu. Miller WH et al. reported that $^{64}$Cu emits lower energy betas and subsequently, has higher self-absorption in the source organ among other beta emitters such as $^{90}Y$, $^{188}Re$, $^{166}Ho$ and $^{149}Pm$ (44). Still, mouse organs are small and they are located close to each other with dimensions comparable to beta ranges, even for beta of lower energy. Therefore, small variation in mice anatomy can lead significant differences in absorbed dose measurement. Since the voxel-based analysis using MC simulation reflects the individual anatomy variation, there is strength in this situation.

Generally, one concern of using single peptide for TRT is high dose delivered to the kidneys. In this study, $^{64}Cu$-GUL show highest absorbed dose in the kidneys among the measured organs.

Data about TRT-related nephrotoxicity are limited (5). There are reports about acute radiation nephritis with uremia and pronounced tubular damage after administration of $^{90}Y$-labeled anticarcinoembryonic antigen Fab fragments (9–15 MBq) and $^{225}Ac$-labeled antibodies (13 kBq) in mice (45, 46). In human, Barone et al. found that the risk of renal dysfunction was increased with a kidney biological effective dose more than 45 Gy in a group of 18 patients treated with $^{90}Y$-DOTATOC (47). Bodei et al. reported a 28 Gy bioeffective dose threshold in patients with preexisting risk factors for renal disease in dosimetry study of 28 patients treated with $^{90}Y$-DOTATOC or $^{177}Lu$ DOTATATE (48).

In clinical studies with PSMA-targeting TRT, Okamoto et al. reported a mean absorbed organ doses of 5.3 $\pm$ 1.6 Gy (0.72 Gy/GBq) for kidneys as a critical organ in patients with $^{177}Lu$-PSMA I&T, which indicates that on average a cumulative activity of 40 GBq of $^{177}Lu$-PSMA I&T is safe when 28 Gy is the dose limit (49). Kabasakal et al. reported a calculated absorbed dose was 0.88 ± 0.40 mGy/MBq for kidneys in patients treated with $^{177}$Lu-PSMA 617 with 30 GBq of dose limit (50). Kuo et al. reported 17.1-fold higher radiation dose to kidneys in a preclinical dosimetry study in mice treated with albumin-conjugated $^{177}$Lu-PSMA 617 derivatives when comparing with those of $^{177}$Lu-PSMA 617 (21).

Compatible with this, the current study also shows higher cumulated activity and higher absorbed dose of the kidneys treated with $^{64}$Cu-albumin-GUL than those treated with $^{64}$Cu-GUL. Despite of minimal renal excretion of albumin-nanoparticle, still it gives higher radiation exposure to the kidneys than single peptide does, probably due to its longer blood circulation.

Liver show the highest absorbed dose among the measured organs when treated with $^{64}$Cu-albumin-GUL. Based on the principle, the organ to whole body radioactivity ratio in mice would be equal to that in human, biodistribution of radiopharmaceuticals obtained in mice has been converted to human biodistribution data by multiplying a ratio of total body weight of the mice/total body weight of adult (51, 52). This formula cannot be applied as it is to calculate absorbed dose because different anatomy and size of organs between mouse and human affecting cross-absorbed dose. But if it is applied only to estimate approximate human absorbed dose to catch a trend, the estimated absorbed doses of $^{64}$Cu-albumin-GUL in the heart wall, lungs, liver and kidneys are 0.033 mGy/MBq, 0.034 mGy/MBq, 0.046 mGy/MBq and 0.037 mGy/MBq, respectively, when 25g was used for total body weight of the mice and 73 kg was used for total body weight of male adult. The estimated absorbed doses of $^{64}$Cu-GUL in those organs were 0.008 mGy/MBq, 0.0009 mGy/MBq, 0.002 mGy/MBq and 0.006 mGy/MBq, respectively, which is minimal compared to those of $^{64}$Cu-albumin-GUL.

In external radiation data, tissue tolerance dose of a 5% rate of complications within 5 years ($TD_{5/5}$) are 45Gy for heart wall, 17.5 Gy for lungs, 30Gy for liver and 23 Gy for kidneys (53). If these are used for dose limit although it is inappropriate that the tissue tolerable dose from external radiation therapy data applies directly to TRT, not liver but lung is a dose-limiting organ among them for $^{64}$Cu-albumin-GUL with average a cumulative activity of 514 GBq.

More important concern when using albumin-nanoparticle is radiation exposure to bone marrow caused by its extended blood retention time. Blood activity is very closely related to absorbed dose to the bone marrow. To measure bone marrow activity, blood or plasma activity concentration is used under the assumption of that extracellular fluid in the marrow spaces has the same activity concentration as plasma, meaning that the red marrow to plasma activity concentration ratio is a constant (54, 55). A standard time-independent value of 0.19 has been conventionally used for red marrow to plasma activity concentration ratio (54, 55). Alternatively, 0.32-0.36 is typically used using whole blood (55, 56). The maximum tolerated dose for red marrow in human are as low as 1-2 Gy, and it is far lower than that of others (17). Taking all of these into account, there is a high probability that bone marrow will become the critical organ rather than liver or lungs when treated with albumin-conjugated nanoparticle.

In dosimetry studies with single peptide GUL, this will be of less concern.

Kabasakal et al. reported that the radiation-absorbed dose delivered to the bone marrow was significantly lower than those of kidneys with the calculated radiation dose to bone marrow of $0.03 \pm 0.01$ mGy/MBq in patients treated with $^{177}$Lu-PSMA 617 (50). Kuo et al. reported that 30.4-fold higher radiation dose to bone marrow with albumin-conjugated $^{177}$Lu-PSMA 617 derivatives was calculated compared with those of $^{177}$Lu-PSMA 617 (21).

In view of TRT, albumin-GUL conjugates have double-sidedness of long blood circulation leading higher tumor uptake and limiting maximum safety dose, which should be taken into consideration for optimal TRT. Recently, it is possible to manipulate *in vivo* biodistribution of albumin nanoplatform as the researchers intended by controlling the DOF attached on the albumin (36). As number of conjugation is increased, liver accumulation is increased and blood pool is decreased. In other words, liver and blood pool has an opposing relationship according to the DOF, probably how fast the particle is eliminated by liver. Therefore, to find the optimal DOF that makes the balance of liver and blood pool activity can be lead to maximize the tolerable dose that patient can be given.

# Conclusions

Comparison of absorbed dose to the normal tissues between single peptide and albumin nanoparticle targeting PSMA was made using voxel-based dosimetry methods. $^{64}$Cu-albumin-GUL can be efficiently synthesized via *click chemistry* technique as a PSMA-targeting nanoplatform with high labeling yield and stability. Along with longer residence time, the calculated absorbed dose of $^{64}$Cu-albumin-GUL was higher than that of $^{64}$Cu-GUL in all organs of the brain, heart wall, liver and kidneys. In view of safety therapeutic radiation dose, albumin-GUL conjugates should be carefully used in human application for optimal TRT.

## References


1. Otte A, Herrmann R, Heppeler A, Behe M, Jermann E, Powell P, et al. Yttrium-90 DOTATOC: first clinical results. European journal of nuclear medicine. 1999;26(11):1439-47.

2. Van Essen M, Krenning EP, Kam BL, De Jong M, Valkema R, Kwekkeboom DJ. Peptide-receptor radionuclide therapy for endocrine tumors. Nature Reviews Endocrinology. 2009;5(7):382.

3. Ersahin D, Doddamane I, Cheng D. Targeted radionuclide therapy. Cancers. 2011;3(4):3838-55.

4. Bobo D, Robinson KJ, Islam J, Thurecht KJ, Corrie SR. Nanoparticle-based medicines: a review of FDA-approved materials and clinical trials to date. Pharmaceutical research. 2016;33(10):2373-87.

5. Vegt E, De Jong M, Wetzels JF, Masereeuw R, Melis M, Oyen WJ, et al. Renal toxicity of radiolabeled peptides and antibody fragments: mechanisms, impact on radionuclide therapy, and strategies for prevention. Journal of nuclear medicine. 2010;51(7):1049-58.

6. An F-F, Zhang X-H. Strategies for preparing albumin-based nanoparticles for multifunctional bioimaging and drug delivery. Theranostics. 2017;7(15):3667.

7. Yousefpour P, Chilkoti AJB, bioengineering. Co-opting biology to deliver drugs. 2014;111(9):1699-716.

8. Anderson CL, Chaudhury C, Kim J, Bronson C, Wani MA, Mohanty SJTii. Perspective–FcRn transports albumin: relevance to immunology and medicine. 2006;27(7):343-8.

9. Chaudhury C, Mehnaz S, Robinson JM, Hayton WL, Pearl DK, Roopenian DC, et al. The major histocompatibility complex–related Fc receptor for IgG (FcRn) binds albumin and prolongs its lifespan. 2003;197(3):315-22.

10. Brandt M, Cardinale J, Giammei C, Guarrochena X, Happl B, Jouini N, et al. Mini-review: Targeted radiopharmaceuticals incorporating reversible, low molecular weight albumin binders. Nuclear medicine and biology. 2019.

11. Carter DC, He X-M, Munson SH, Twigg PD, Gernert KM, Broom MB, et al. Three-dimensional structure of human serum albumin. 1989;244(4909):1195-8.

12. Green M, Manikhas G, Orlov S, Afanasyev B, Makhson A, Bhar P, et al. Abraxane®, a novel Cremophor®-free, albumin-bound particle form of paclitaxel for the treatment of advanced non-small-cell lung cancer. Annals of Oncology. 2006;17(8):1263-8.

13. Miele E, Spinelli GP, Miele E, Tomao F, Tomao S. Albumin-bound formulation of paclitaxel (Abraxane® ABI-007) in the treatment of breast cancer. International journal of nanomedicine. 2009;4:99.

14. Snyder W, Ford M, Warner G, Watson SJNYSoNM. MIRD pamphlet no. 11: S, absorbed dose per unit cumulated activity for selected radionuclides and organs. 1975.

15. Gupta A, Lee MS, Kim JH, Park S, Park HS, Kim SE, et al. Preclinical voxel-based dosimetry through GATE Monte Carlo simulation using PET/CT imaging of mice. 2019;64(9):095007.

16. Bryan JN, Jia F, Mohsin H, Sivaguru G, Anderson CJ, Miller WH, et al. Monoclonal antibodies for copper-64 PET dosimetry and radioimmunotherapy.

Cancer biology & therapy. 2011;11(12):1001-7.

17. Avila-Rodriguez M, Rios C, Carrasco-Hernandez J, Manrique-Arias J, Martinez-Hernandez R, García-Pérez F, et al. Biodistribution and radiation dosimetry of [64 Cu] copper dichloride: first-in-human study in healthy volunteers. EJNMMI research. 2017;7(1):98.

18. Bray F, Ferlay J, Soerjomataram I, Siegel RL, Torre LA, Jemal A. Global cancer statistics 2018: GLOBOCAN estimates of incidence and mortality worldwide for 36 cancers in 185 countries. CA: a cancer journal for clinicians. 2018;68(6):394-424.

19. Jung K-W, Won Y-J, Kong H-J, Lee ES. Cancer statistics in Korea: incidence, mortality, survival, and prevalence in 2015. Cancer research and treatment: official journal of Korean Cancer Association. 2018;50(2):303.

20. Pinto JT, Suffoletto BP, Berzin TM, Qiao CH, Lin S, Tong WP, et al. Prostate-specific membrane antigen: a novel folate hydrolase in human prostatic carcinoma cells. Clinical Cancer Research. 1996;2(9):1445-51.

21. Kuo H-T, Merkens H, Zhang Z, Uribe CF, Lau J, Zhang C, et al. Enhancing treatment efficacy of 177Lu-PSMA-617 with the conjugation of an albumin-binding motif: Preclinical dosimetry and endoradiotherapy studies. Molecular pharmaceutics. 2018;15(11):5183-91.

22. Silver DA, Pellicer I, Fair WR, Heston W, Cordon-Cardo C. Prostate-specific membrane antigen expression in normal and malignant human tissues. Clinical cancer research. 1997;3(1):81-5.

23. Lütje S, Heskamp S, Cornelissen AS, Poeppel TD, van den Broek SA,

Rosenbaum-Krumme S, et al. PSMA ligands for radionuclide imaging and therapy of prostate cancer: clinical status. Theranostics. 2015;5(12):1388.

24. Barrio M, Fendler WP, Czernin J, Herrmann K. Prostate specific membrane antigen (PSMA) ligands for diagnosis and therapy of prostate cancer. Expert review of molecular diagnostics. 2016;16(11):1177-88.

25. Eiber M, Fendler WP, Rowe SP, Calais J, Hofman MS, Maurer T, et al. Prostate-specific membrane antigen ligands for imaging and therapy. J Nucl Med. 2017;58(Suppl 2):67S-76S.

26. Weineisen M, Schottelius M, Simecek J, Baum RP, Yildiz A, Beykan S, et al. 68Ga-and 177Lu-labeled PSMA I&T: optimization of a PSMA-targeted theranostic concept and first proof-of-concept human studies. Journal of Nuclear Medicine. 2015;56(8):1169-76.

27. Heck MM, Retz M, D'Alessandria C, Rauscher I, Scheidhauer K, Maurer T, et al. Systemic radioligand therapy with 177Lu labeled prostate specific membrane antigen ligand for imaging and therapy in patients with metastatic castration resistant prostate cancer. The Journal of urology. 2016;196(2):382-91.

28. Rahbar K, Ahmadzadehfar H, Kratochwil C, Haberkorn U, Schäfers M, Essler M, et al. German multicenter study investigating 177Lu-PSMA-617 radioligand therapy in advanced prostate cancer patients. Journal of Nuclear Medicine. 2017;58(1):85-90.

29. Dietlein M, Kobe C, Kuhnert G, Stockter S, Fischer T, Schomäcker K, et al. Comparison of [18 F] DCFPyL and [68 Ga] Ga-PSMA-HBED-CC for PSMA-PET imaging in patients with relapsed prostate cancer. Molecular Imaging and

Biology. 2015;17(4):575-84.

30. Giesel FL, Hadaschik B, Cardinale J, Radtke J, Vinsensia M, Lehnert W, et al. F-18 labelled PSMA-1007: biodistribution, radiation dosimetry and histopathological validation of tumor lesions in prostate cancer patients. European journal of nuclear medicine and molecular imaging. 2017;44(4):678-88.

31. Chen Y, Foss CA, Byun Y, Nimmagadda S, Pullambhatla M, Fox JJ, et al. Radiohalogenated prostate-specific membrane antigen (PSMA)-based ureas as imaging agents for prostate cancer. Journal of medicinal chemistry. 2008;51(24):7933-43.

32. Umbricht CA, Benešová M, Schibli R, Müller C. Preclinical development of novel PSMA-targeting radioligands: modulation of albumin-binding properties to improve prostate cancer therapy. Molecular pharmaceutics. 2018;15(6):2297-306.

33. Umbricht CA, Benešová M, Hasler R, Schibli R, van der Meulen NP, Müller C. Design and Preclinical Evaluation of an Albumin-Binding PSMA Ligand for 64Cu-Based PET Imaging. Molecular pharmaceutics. 2018;15(12):5556-64.

34. Benešová M, Umbricht CA, Schibli R, Müller C. Albumin-binding PSMA ligands: optimization of the tissue distribution profile. Molecular pharmaceutics. 2018;15(3):934-46.

35. Moon S-H, Hong MK, Kim YJ, Lee Y-S, Lee DS, Chung J-K, et al. Development of a Ga-68 labeled PET tracer with short linker for prostate-specific membrane antigen (PSMA) targeting. Bioorganic & medicinal chemistry. 2018;26(9):2501-7.

36. Park JY, Song MG, Kim10 WH, Kim KW, Lodhi NA, Choi JY, et al.

Versatile and Finely Tuned Albumin Nanoplatform based on Click Chemistry. 2019;9(12):3398-409.

37. Jan S, Santin G, Strul D, Staelens S, Assie K, Autret D, et al. GATE: a simulation toolkit for PET and SPECT. Phys Med Biol. 2004;49(19):4543-61.

38. Agostinelli S, Allison J, Amako Ka, Apostolakis J, Araujo H, Arce P, et al. GEANT4—a simulation toolkit. Nuclear instruments and methods in physics research section A: Accelerators, Spectrometers, Detectors and Associated Equipment. 2003;506(3):250-303.

39. Matsumoto M, Nishimura T. Mersenne twister: a 623-dimensionally equidistributed uniform pseudo-random number generator. ACM Transactions on Modeling and Computer Simulation (TOMACS). 1998;8(1):3-30.

40. Gupta A, Lee MS, Kim JH, Park S, Park HS, Kim SE, et al. Preclinical voxel-based dosimetry through GATE Monte Carlo simulation using PET/CT imaging of mice. Physics in medicine and biology. 2019.

41. Sarrut D, Bardiès M, Boussion N, Freud N, Jan S, Létang JM, et al. A review of the use and potential of the GATE Monte Carlo simulation code for radiation therapy and dosimetry applications. Medical physics. 2014;41(6Part1).

42. Woo S-K, Jang SJ, Seo M-J, Park JH, Kim BS, Kim EJ, et al. Development of 64Cu-NOTA-Trastuzumab for HER2 Targeting: A Radiopharmaceutical with Improved Pharmacokinetics for Human Studies. 2019;60(1):26-33.

43. Xie T, Zaidi HJPiM, Biology. Monte Carlo-based evaluation of S-values in mouse models for positron-emitting radionuclides. 2012;58(1):169.

44. Miller WH, Hartmann-Siantar C, Fisher D, Descalle M-A, Daly T,

Lehmann J, et al. Evaluation of beta-absorbed fractions in a mouse model for 90Y, 188Re, 166Ho, 149Pm, 64Cu, and 177Lu radionuclides. 2005;20(4):436-49.

45. Behr TM, Sharkey RM, Sgouros G, Blumenthal RD, Dunn RM, Kolbert K, et al. Overcoming the nephrotoxicity of radiometal-labeled immunoconjugates: improved cancer therapy administered to a nude mouse model in relation to the internal radiation dosimetry. Cancer: Interdisciplinary International Journal of the American Cancer Society. 1997;80(S12):2591-610.

46. Jaggi JS, Seshan SV, McDevitt MR, LaPerle K, Sgouros G, Scheinberg DA. Renal Tubulointerstitial Changes after Internal Irradiation with α-Particle–Emitting Actinium Daughters. Journal of the American Society of Nephrology. 2005;16(9):2677-89.

47. Barone R, Borson-Chazot F, Valkema R, Walrand S. Patient-specific dosimetry in predicting renal toxicity with^ sup 90^ Y-DOTATOC: relevance of kidney volume and dose rate in finding a dose-effect relationship. The Journal of Nuclear Medicine. 2005;46:99S.

48. Bodei L, Cremonesi M, Ferrari M, Pacifici M, Grana CM, Bartolomei M, et al. Long-term evaluation of renal toxicity after peptide receptor radionuclide therapy with 90 Y-DOTATOC and 177 Lu-DOTATATE: the role of associated risk factors. European journal of nuclear medicine and molecular imaging. 2008;35(10):1847-56.

49. Okamoto S, Thieme A, Allmann J, D'Alessandria C, Maurer T, Retz M, et al. Radiation dosimetry for 177Lu-PSMA I&T in metastatic castration-resistant prostate cancer: absorbed dose in normal organs and tumor lesions. Journal of

Nuclear Medicine. 2017;58(3):445-50.

50. Kabasakal L, AbuQbeitah M, Aygün A, Yeyin N, Ocak M, Demirci E, et al. Pre-therapeutic dosimetry of normal organs and tissues of 177 Lu-PSMA-617 prostate-specific membrane antigen (PSMA) inhibitor in patients with castration-resistant prostate cancer. European journal of nuclear medicine and molecular imaging. 2015;42(13):1976-83.

51. Josefsson A, Nedrow JR, Park S, Banerjee SR, Rittenbach A, Jammes F, et al. Imaging, biodistribution, and dosimetry of radionuclide-labeled PD-L1 antibody in an immunocompetent mouse model of breast cancer. 2016;76(2):472-9.

52. Natarajan A, Patel CB, Habte F, Gambhir SSJSr. Dosimetry Prediction for Clinical Translation of 64 Cu-Pembrolizumab ImmunoPET Targeting Human PD-1 Expression. 2018;8(1):633.

53. Meredith R, Wessels B, Knox S, editors. Risks to normal tissues from radionuclide therapy. Seminars in nuclear medicine; 2008: Elsevier.

54. Sgouros GJJonmop, Society of Nuclear Medicine. Bone marrow dosimetry for radioimmunotherapy: theoretical considerations. 1993;34(4):689-94.

55. Schwartz J, Humm JL, Divgi CR, Larson SM, O'Donoghue JAJJonm. Bone marrow dosimetry using 124I-PET. 2012;53(4):615-21.

56. Sgouros G, Stabin M, Erdi Y, Akabani G, Kwok C, Brill AB, et al. Red marrow dosimetry for radiolabeled antibodies that bind to marrow, bone, or blood components. 2000;27(9):2150-64.

# 국 문 초 록

# PET 영상 기반 생체 분포 및 흡수 선량 측정을 통한 $^{64}$Cu-GUL 와 $^{64}$Cu-Albumin-GUL 의 비교

이은성

서울대학교

융합과학기술대학원

분자의학 및 바이오제약학과

전립선특이막항체 표적 핵종 치료가 전립선 암 치료의 최첨단 임상 분야에 도입되었다. 표적 핵종 치료의 효과는 주로 종양과 정상 조직의 총 흡수 선량에 달려 있다. 따라서, 종양 치사량 이상이고 최대 안전 선량 이하인 방사 선량의 범위가 최대한 정확하게 결정되어야 한다. 장기 수준의 선량 측정과 관련된 여러 가지 제한 때문에, 표적 핵종 치료 동안 보다 정확한 흡수 선량을 평가하기 위해서는 복셀 기반의 선량 측정법이 필수적이게 되었다. 본 연구의 주요 목적은 복셀 기반의

선량 측정법을 사용하여 전립선특이막항체 표적 펩타이드와 알부민 나노 입자의 정상조직에 대한 방사선량을 비교하는 것이다.

본 연구에서는 전립선특이막항체를 표적하는 방사선 표지 펩타이드 ($^{64}$Cu−GUL)와 알부민 나노 입자 ($^{64}$Cu−albumin−GUL)를 합성하고, 정상 쥐의 PET/CT 영상을 가지고 직접 GATE MC 시뮬레이션방법을 이용하여 복셀 기반 선량 측정을 수행하였다.

$^{64}$Cu−albumin−GUL이 $^{64}$Cu−GUL과 비교하여 뇌, 심장벽, 폐, 간 그리고 신장의 흡수 선량이 모두 높았다. $^{64}$Cu−GUL은 주로 신장에 축적되었으며, $^{64}$Cu−albumin−GUL는 간에 축적되었다. 혈액 저류 시간 역시 $^{64}$Cu−albumin−GUL 가 $^{64}$Cu−GUL 보다 높았다.

단일 펩타이드 $^{64}$Cu−GUL은 신장의 방사선량이 높고, 알부민 나노 입자 $^{64}$Cu−albumin−GUL은 긴 혈액 순환으로 인해 정상조직에 대한 방사선량을 전반적으로 증가시키므로 최적의 표적 핵종 치료 계획을 위해서는 이를 고려해야 할 것이다.

주요어: 복셀 기반 선량 측정법, GATE, $^{64}$Cu−GUL, $^{64}$Cu−알부민−GUL, PET/CT, 전립선특이막항체

학번: 2010−24240